Journal of South American Earth Sciences 45 (2013) 24–41

Contents lists available at SciVerse ScienceDirect

Journal of South American Earth Sciences

journal homepage: www.elsevier.com/locate/jsames

# Middle Miocene near trench volcanism in northern Colombia: A record of slab tearing due to the simultaneous subduction of the Caribbean Plate under South and Central America?

M. Lara [a,*], A. Cardona [b], G. Monsalve [c], J. Yarce [c], C. Montes [d], V. Valencia [e], M. Weber [c], F. De La Parra [f], D. Espitia [f], M. López-Martínez [g]

[a] Corporación Geológica Ares, Calle 44A # 53-96, Bogotá, Colombia
[b] Escuela de Procesos y Energía, Universidad Nacional de Colombia, Medellín, Colombia
[c] Escuela de Geociencias y Medio Ambiente, Universidad Nacional de Colombia, Medellín, Colombia
[d] Geociencias, Universidad de los Andes, Bogotá, Colombia
[e] School of Earth and Environmental Sciences, Washington State University, Pullman, USA
[f] Instituto Colombiano del Petróleo, Bucaramanga (ICP), Colombia
[g] Div de Ciencias de la Tierra, CICESE, Carretera Ensenada Tijuana No 3918, Zona Playitas, Ensenada Baja California, México CP 22860, Mexico

ARTICLE INFO

*Article history:*
Received 1 September 2012
Accepted 17 December 2012

*Keywords:*
Miocene
Volcanism
Subduction
Caribbean plate
Slab tear

ABSTRACT

Field, geochemical, geochronological, biostratigraphical and sedimentary provenance results of basaltic and associated sediments northern Colombia reveal the existence of Middle Miocene (13–14 Ma) mafic volcanism within a continental margin setting usually considered as amagmatic. This basaltic volcanism is characterized by relatively high $Al_2O_3$ and $Na_2O$ values (>15%), a High-K calc-alkaline affinity, large ion lithophile enrichment and associated Nb, Ta and Ti negative anomalies which resemble High Al basalts formed by low degree of asthenospheric melting at shallow depths mixed with some additional slab input. The presence of pre-Cretaceous detrital zircons, tourmaline and rutile as well as biostratigraphic results suggest that the host sedimentary rocks were deposited in a platform setting within the South American margin. New results of P-wave residuals from northern Colombia reinforce the view of a Caribbean slab subducting under the South American margin.

The absence of a mantle wedge, the upper plate setting, and proximity of this magmatism to the trench, together with geodynamic constraints suggest that the subducted Caribbean oceanic plate was fractured and a slab tear was formed within the oceanic plate. Oceanic plate fracturing is related to the splitting of the subducting Caribbean Plate due to simultaneous subduction under the Panama-Choco block and northwestern South America, and the fast overthrusting of the later onto the Caribbean oceanic plate.



## 1. Introduction

Near-trench volcanism in convergent margins may be related to plate flexure in the downgoing oceanic plate (Hirano et al., 2006), upper plate transtensional rifting (Davis et al., 2010), slab tearing and associated roll back (Gasparon, 2009; Wortel et al., 2009; Yamamoto and Hoang, 2009) or the subduction of an oceanic spreading center (Thorkelson, 1996; Madsen et al., 2006).

Resolving each of these scenarios in younger or ancient orogens is crucial for understanding the long term tectonic evolution of convergent margins and related effects of variable convergence relations in the magmatic record of the upper plate (Cawood et al., 2009).

Cenozoic tectonic reconstructions and geophysical data have suggested that the interactions of the southern margin of the Caribbean plate against northern South America is characterized by an oblique and slow E-SE plate convergence and flat subduction configuration (Van der Hilst and Mann, 1994; Taboada et al., 2000; Corredor, 2003; Cortés y Angelier, 2005; Weber et al., 2001; Vargas et al., 2010; Mantilla-Pimiento et al., 2009; Bernal et al., 2012).

* Corresponding author. Calle 1 N 43D30, apto 606, Envigado, Colombia.
*E-mail address:* marioelarao@gmail.com (M. Lara).

0895-9811/$ – see front matter © 2013 Elsevier Ltd. All rights reserved.
http://dx.doi.org/10.1016/j.jsames.2012.12.006

Associated to this plate convergence a large sedimentary accretionary prism (South Caribbean Deformed Belt: SCDB) has been growing in the Caribbean-South America plate margin since the Eocene (Case et al., 1974; Duque-Caro, 1984, Fig. 1A,B). Due to the slow plate convergence and/or flat slab subduction the continental margin has been considered as amagmatic, with volcanism restricted to transtensional pull-apart basins such as the Falcon Basin in Venezuela (Muessig, 1984).

In this contribution we integrate field, geochemical, geochronological and biostratigraphical data to document the existence of two new exposures of volcanic rocks, in the town of Puerto Escondido-Córdoba and Necoclí-Antioquia (between the hamlet of Mulatos and Zapata), associated to Miocene sediments in the SCDB (Fig. 1C). These results together with new analysis of P-wave residuals of northern Colombia and regional tectonic synthesis are used to discuss the existence of a Middle Miocene near trench magmatism in northern Colombia, associated with the formation of a tear in the subducting Caribbean oceanic plate. The fracturing of the oceanic plate is considered as a major consequence of the subduction of the Caribbean plate under two different margins, the South American and Central American isthmus. This setting follows the collision of the Panama-Choco block against the South American margin and the associated overthrusting of the later over the Caribbean plate.

## 2. Geological setting

The Southern Caribbean Plate Boundary in northern Colombia is characterized by a series of discontinuous ranges of deformed marine to transitional sedimentary belts and isolated Pre-Eocene crystalline massifs (Fig. 1A,B).

Both the basement of the deformed sedimentary belts and the northernmost segments of the crystalline massifs include the remnants of Cretaceous intra-oceanic basement accreted to the continental margin between the Maastrichtian and the Paleocene (Duque-Caro, 1984; Kerr et al., 1997; Weber et al., 2009, Cardona et al., 2010; Villagómez et al., 2011).

This older accretionary event is linked to the northeastern advance and collision of the allochthonous Caribbean plate from a Pacific position (Burke, 1988; Pindell et al., 1998, 2005; Pindell and Kennan, 2009). Subsequent Cenozoic oblique convergence between the Caribbean and the South American plates has ended in the growth of several transpressional orogens, the formation and lateral migration of different sedimentary accretionary prisms, and the growth of different rotational and pull-apart basins (Toto and Kellogg, 1992; Duque-Caro, 1984; Macellari, 1984; Pindell et al., 1998; Flinch, 2003; Flinch et al., 2003; Montes et al., 2010).

The northernmost and youngest of these sedimentary prisms already presented as the SCDB (Fig. 1A,B; Case, 1974) extends along the offshore margin of the northern South American Plate with thickness up to 5000 m. Its deformational history and tectonic position have been interpreted as a major expression of an accretionary prism that grew due to the plate convergence between the Caribbean and South American plates (Toto and Kellogg, 1992; Duque-Caro, 1984; Flinch, 2003; Flinch et al., 2003). In northern Colombia the onshore exposure of this highly deformed belt include Oligo-Pliocene sediments grouped in the Sinú belt (Fig. 1B, Duque-Caro, 1984). This belt was deposited in transitional to marine environments and was deformed during the Pliocene-Pleistocene associated with significant mud diapirism (Toto and Kellogg, 1992; Duque-Caro, 1984; Cerón et al., 2007; Mantilla-Pimiento et al., 2009).

Modern geodynamic configuration of the plate boundary zone in the northern Colombia is characterized by oblique east-southeast plate convergence at slow rates of ~20 mm/y (Kellogg and Vega, 1995; Taboada et al., 2000; Perez et al., 2001; Weber et al., 2001; Trenkamp et al., 2002; Colmenares and Zoback, 2003). Although still controversial, geophysical constraints suggested the existence of a very flat subduction angle (~12–19°) of the Caribbean slab beneath the continent in Northwestern Colombia (Van Der Hilst and Mann, 1994; Corredor, 2003; Cortés y Angelier, 2005; Vargas et al., 2010; Mantilla-Pimiento et al., 2009; Bernal et al., 2012).

Seismicity defines a Wadati–Benioff zone dipping southward beneath the Panama block, indicating the presence of active subduction along the trailing edge of the Caribbean plate, with earthquakes penetrating as far as 80 km depth and 150 km south of the trench (Camacho et al., 2010). This tectonic configuration may have started at least since the Early Miocene when increased convergence velocity between the Americas may have caused the onset of underthrusting of the Caribbean oceanic crust below the South America borderland with East–West migration of the Caribbean plate (Müller et al., 1999), which may have also brought the Panama block in collision course with northwestern South America (Farris et al., 2011; Montes et al., 2012a,b).

## 3. Methods

### 3.1. Petrography and heavy minerals

Seventeen representative samples were selected for petrographic analysis, including massive volcanic rocks (eight samples), siliciclastic sediments associated (five samples) and volcanic blocks from peperitic facies (four samples) which are considered as rocks formed essentially in situ by disintegration of magma intruding and mingling with unconsolidated or poorly consolidated, typically wet sediments (White et al., 2000; Skilling et al., 2002).

Sandstones were point counted to determine their composition and provenance, following framework analysis after Folk (1980) and Dickinson (1985). Three sandstone samples associated with the basalts were selected for heavy mineral analysis. Heavy minerals were concentrated with sodium poly tungsten (LST®) at a density of 2.9 g/cm$^3$ and mounted in a resin (Meltmount®) with a refraction index of 1.539. Data analysis was performed by the counting and identification of 350 grains following the Ribbon-Counting method (Mange and Maurer, 1992).

### 3.2. Ar–Ar geochronology

$^{40}$Ar–$^{39}$Ar analyses of plagioclase were carried out on three volcanic rocks samples.

Minerals were pretreated and concentrated by standard laboratory techniques and later selected by handpicking under a binocular microscope. Analytical results are presented in Table 1.

Two samples from the Puerto Escondido outcrop (Fig. 1C) were selected for analysis. One sample from the massive volcanic facies and the other a volcanic block within the peperitic facies. Ar–Ar step heating analysis were performed at the Geochronology Laboratory of the Departamento de Geología, CICESE, Baja California, Mexico. The argon isotope experiments were conducted on mineral grains with a coherent Ar-ion Innova 370 laser extraction system on line with a VG5400 mass spectrometer. All the samples and irradiation monitors were irradiated in the U-enriched research reactor of the University of McMaster in Hamilton, Canada, at position 5C in capsule CIC-66 for 10hr. To block thermal neutrons, the capsule was covered with a cadmium liner during irradiation. As irradiation monitors, aliquots of standard FCT-2 sanidine (27.84 ± 0.04 Ma) were irradiated alongside the samples and distributed among them to determine the neutron flux variations. Upon irradiation the monitors were fused in one step

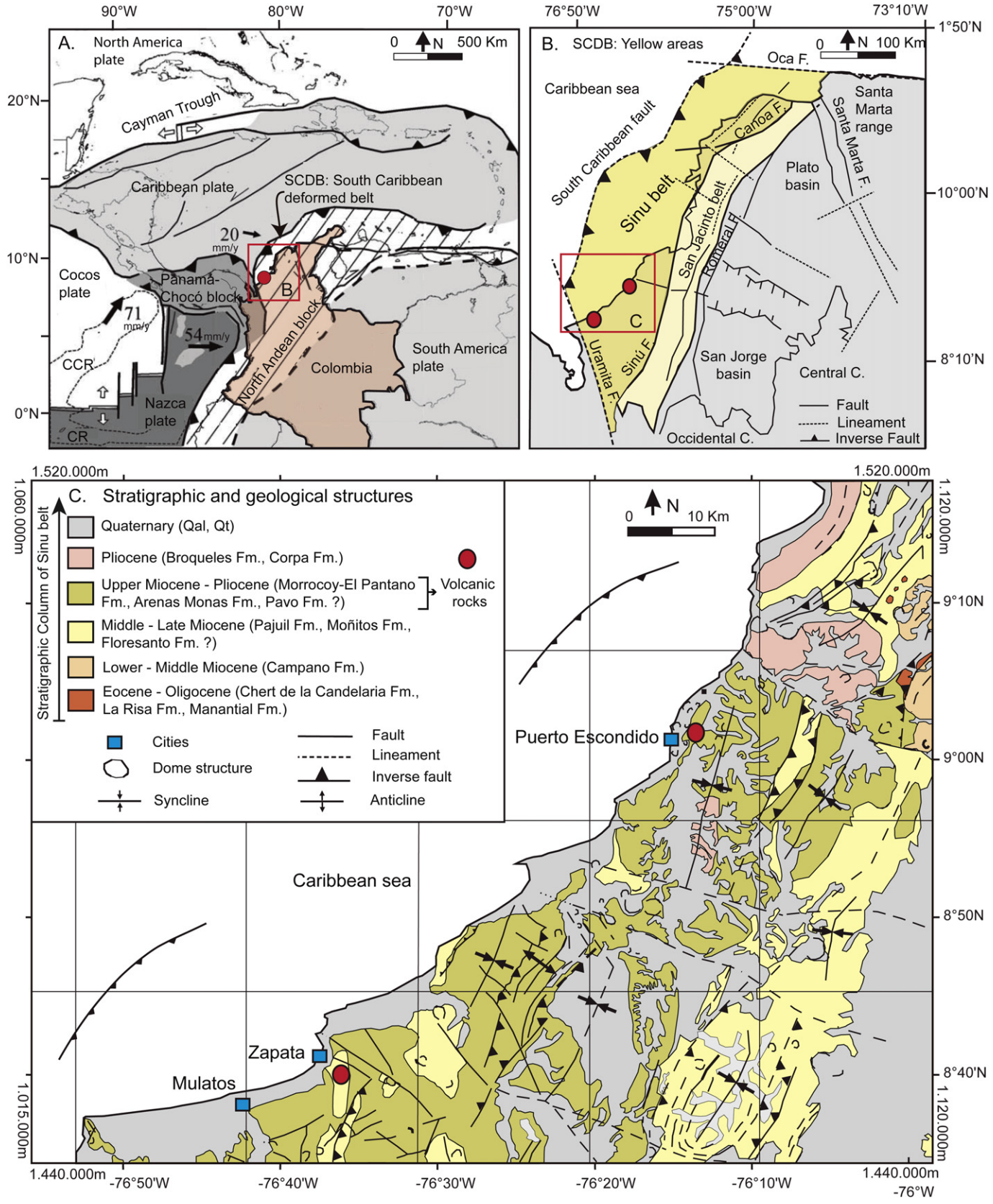


**Fig. 1.** Location of the volcanic rocks from Sinú belt; A. Current configuration of the Caribbean plate (Modified from Cortés and Angelier, 2005); B. Modern tectonic framework of northwestern Colombia and location of the South Caribbean Deformed Belt including the Sinú and San Jacinto belts (modified from Duque-Caro, 1984; Geotec, 2003; Flinch, 2003; Guzmán, 2007); C. Regional stratigraphy and geology of the volcanic exposures (modified from Gómez et al., 2007).

**Table 1**
A. $^{40}Ar/^{39}Ar$ ages of the studied basalts; B–C. Ar–Ar step-heating data sample from Puerto Escondido outcrop. D. Ar–Ar step-heating data sample from Necoclí outcrop, between the hamlet of Mulatos and Zapata.

A)

| Sample | Rock/Material dated | Outcrop | Outcrop Coordinate | Plateau age (Ma) | Isochron age (Ma) | $(^{40}Ar/^{36}Ar)i$ | MSWD isochron/*n* |
|---|---|---|---|---|---|---|---|
| MLC021M2[a] | Basalt/plg | Puerto Escondido | 09°02′N −76°14′W | 13.24 ± 0.64[c] | 14.0 ± 2.0 | 308 ± 67 | 2.1/9 |
| MLC019M5[b] | Basalt/plg | | | 13.43 ± 0.40[d] | 12.88 ± 0.67 | 380 ± 49 | 1.2/6 |
| BA06-VB[a] | Basalt/plg | Necoclí | 08°40′N −76°36′W | 14.40 ± 0.30[e] | 14.3 ± 0.3 | 312 ± 10 | 0.14/9 |

B)

Plagioclase MLC021M2

| Pwr | $^{39}Ar \times 10^{-6}$ | $F^{39}Ar$ | $^{40}Ar^*/^{39}Ar_K$ | Age in Ma | | | $\%^{40}Ar^*$ | $^{40}Ar/^{36}Ar$ | $^{37}Ar_{Ca}/^{39}Ar_K$ |
|---|---|---|---|---|---|---|---|---|---|
| 1.50 | 44.099 | 0.1107 | 0.09 ± 0.67 | 0.60 ± 4.45 | a | [f] | 0.32 | 296 | 6.78 |
| 2.90 | 38.831 | 0.0975 | 3.01 ± 0.44 | 19.99 ± 2.91 | b | | 72.32 | 1068 | 7.19 |
| 4.60 | 40.087 | 0.1007 | 2.15 ± 0.37 | 14.30 ± 2.44 | c | | 52.52 | 622 | 7.17 |
| 5.80 | 84.241 | 0.2115 | 1.77 ± 0.19 | 11.82 ± 1.23 | d | | 46.57 | 553 | 7.53 |
| 12.00 | 190.960 | 0.4795 | 2.06 ± 0.12 | 13.72 ± 0.79 | e | | 71.97 | 1054 | 7.76 |
| 1.00 | 18.717 | 0.0390 | 2.87 ± 6.55 | 19.07 ± 43.33 | f | [f] | 4.31 | 309 | 5.21 |
| 2.50 | 73.252 | 0.1526 | 1.27 ± 0.26 | 8.50 ± 1.70 | g | [f] | 15.02 | 348 | 7.20 |
| 4.50 | 50.019 | 0.1042 | 2.06 ± 0.25 | 13.73 ± 1.64 | h | | 52.23 | 619 | 7.07 |
| 5.50 | 36.113 | 0.0752 | 2.66 ± 0.39 | 17.68 ± 2.60 | i | | 61.96 | 777 | 7.10 |
| 7.50 | 203.264 | 0.4234 | 2.16 ± 0.05 | 14.40 ± 0.30 | j | | 61.51 | 768 | 7.48 |
| 10.50 | 63.339 | 0.1319 | 2.49 ± 0.16 | 16.54 ± 1.08 | k | | 78.16 | 1353 | 7.45 |
| 13.00 | 35.350 | 0.0736 | 2.06 ± 0.23 | 13.70 ± 1.55 | l | | 58.60 | 714 | 7.38 |

Integrated results

| $^{39}Ar \times 10^{-6}$ | $^{40}Ar^*/^{39}Ar_K$ | Age in Ma | $\%^{40}Ar^*$ | $^{40}Ar/^{36}Ar$ | $^{37}Ar_{Ca}/^{39}Ar_K$ |
|---|---|---|---|---|---|
| 398.2 | 1.88 ± 0.12 | 12.54 ± 0.78 | 30.67 | 426.22 | 7.49 |
| 480.1 | 2.12 ± 0.26 | 14.09 ± 1.75 | 31.17 | 429.29 | 7.27 |

C)

Plagioclase MLC019M5

| Pwr | $^{39}Ar \times \mathbf{10^{-6}}$ | $F^{39}Ar$ | $^{40}Ar^*/^{39}Ar_K$ | Age in Ma | | $\%^{40}Ar^*$ | $^{40}Ar/^{36}Ar$ | $^{37}Ar_{Ca}/^{39}Ar_K$ |
|---|---|---|---|---|---|---|---|---|
| 1.16 | 17.421 | 0.0604 | 3.74 ± 0.74 | 24.83 ± 4.89 | a | 36.74 | 467 | 7.12 |
| 2.50 | 32.079 | 0.1112 | 2.36 ± 0.24 | 15.70 ± 1.59 | b | 80.11 | 1485 | 7.33 |
| 4.50 | 30.234 | 0.1048 | 2.03 ± 0.24 | 13.50 ± 1.60 | c | 86.58 | 2202 | 7.51 |
| 5.50 | 63.394 | 0.2197 | 1.81 ± 0.14 | 12.08 ± 0.92 | d | 76.98 | 1284 | 7.69 |
| 6.00 | 80.181 | 0.2778 | 2.09 ± 0.08 | 13.92 ± 0.50 | e | 90.54 | 3125 | 7.45 |
| 8.00 | 65.271 | 0.2262 | 1.96 ± 0.15 | 13.04 ± 0.98 | f | 76.86 | 1277 | 7.63 |

Integrated results

| $^{39}Arx10^{-6}$ | $^{40}Ar^*/^{39}Ar_K$ | Age in Ma | $\%^{40}Ar^*$ | $^{40}Ar/^{36}Ar$ | $^{37}Ar_{Ca}/^{39}Ar_K$ |
|---|---|---|---|---|---|
| 288.6 | 2.12 ± 0.08 | 14.13 ± 0.51 | 72.63 | 1080 | 7.52 |

D)

Plagioclase BA06-VB

| ID | Watts | Ca/K | Cl/K | $^{36}Ar/^{39}Ar$ | $\%^{36}Ar(Ca)$ | $^{40}Ar^*/^{39}Ar_K$ | Mol$^{39}Ar$ | %step | Cum.% | $\%^{40}Ar^*$ | Age in Ma |
|---|---|---|---|---|---|---|---|---|---|---|---|
| a | 2 | 11.0141 | 0.0058 | 0.4587 | 0.4 | 9.6842 | 0.0139 | 0.4 | 0.4 | 6.7 | 27.26 ± 17.45 |
| b | 4 | 12.9825 | 0.0026 | 0.0295 | 6.6 | 5.7373 | 0.1518 | 3.8 | 4.2 | 41.2 | 16.20 ± 1.10 |
| c | 6 | 14.4305 | 0.0098 | 0.0047 | 45.3 | 5.1506 | 0.286 | 7.3 | 11.5 | 87 | 14.55 ± 0.78 |
| d | 8 | 13.9277 | 0.0049 | 0.0043 | 48.8 | 5.0519 | 0.522 | 13.2 | 24.7 | 88.5 | 14.27 ± 0.31 |
| e | 10 | 13.1088 | 0.0034 | 0.0037 | 53.1 | 5.0685 | 0.845 | 21.4 | 46.1 | 90.8 | 14.31 ± 0.32 |
| f | 14 | 14.5845 | 0.0005 | 0.0034 | 63.6 | 5.0844 | 0.7066 | 17.9 | 64 | 93.2 | 14.36 ± 0.33 |
| g | 18 | 12.6633 | 0.0006 | 0.0024 | 78.1 | 5.0970 | 0.9484 | 24 | 88.1 | 97 | 14.40 ± 0.19 |
| h | 22 | 13.8534 | 0.0005 | 0.0032 | 63.8 | 4.9426 | 0.2675 | 6.8 | 94.9 | 93.4 | 13.96 ± 0.91 |
| i | 30 | 14.4943 | 0.0075 | 0.0087 | 55.9 | 5.0864 | 0.2030 | 5.1 | 100 | 90.9 | 14.37 ± 1.04 |
| Integrated age | | | | | | | | | | | 14.4 ± 0.4 (MWSD = 0.14) |
| Plateau age | | | | | | | | 100% | | | 14.4 ± 0.3 (MWSD = 0.46) |

-The plateau age from sample MLC021M2 was calculated with the weighted mean of fractions c to e.
-The plateau age from sample MLC019M5 was calculated with the weighted mean of fractions c to f.
[a] Massive porphyritic basalts.
[b] Volcanic block from the peperitic facies.
[c] 79.18% of $^{39}Ar$ released in 3 consecutive fractions, MSWD plateau = 0.94.
[d] 82.84% of $^{39}Ar$ released in 4 consecutive fractions, MSWD plateau = 1.08.
[e] 50% min-100% of $^{39}Ar$ released in 3 consecutive fractions, MSWD plateau = 0.46.
[f] Fractions ignored in the isochron given in the figure.

while the samples were step-heated. The argon isotopes were corrected for blank, mass discrimination, radioactive decay of $^{37}Ar$, $^{39}Ar$ and atmospheric contamination. For the Ca neutron interference reactions, the factors given by Masliwec (1984) were used. In processing the data, the decay constants recommended by Steiger and Jäger (1977) were applied. The equations reported by York et al. (2004) were used in all the straight line fitting routines of the argon data reduction.

$^{40}Ar-^{39}Ar$ analyses in plagioclase also was carried out on a massive basalt sample from Necoclí outcrop (Fig. 1C; between the hamlet of Mulatos and Zapata). This was performed at the Geochronology Laboratory of the Servicio Nacional de Geología y Minería (SERNAGEOMIN), Chile.

The plateau age was calculated from the weighted mean of consecutive fractions that were in agreement within $1\sigma$. The error in the plateau, and in the integrated and isochron ages includes the scatter in the irradiation monitors. The analytical precision is reported as one standard deviation ($1\sigma$).

For each sample the relevant $^{40}Ar-^{39}Ar$ data for all the experiments is presented, and includes the results for the individual steps and the integrated ages.

### 3.3. Biostratigraphy

A total of six samples were collected and processed for palynological and micropalentological (foraminifera) analysis following the standard procedure described in Traverse (2007) for palynology whereas for micropaleontological purposes samples were disaggregated in water and washed repeatedly through a set of sieves (149 and 63 μm mesh) and then the residual material was dried in an oven at 40 °C. Light microscopy and binocular stereo microscopy were used to examine the palynological and micropaleontological content of the samples, respectively. At least 200 palynomorphs were counted in each preparation and all foraminifera present in the 250 μm, 125 μm and 63 μm fractions were picked from the residual material. The morphological characteristics of the palynomorphs were compared with descriptions published in the literature (Jaramillo et al., 2010; Geermerad et al., 1968; Hoorn et al., 1987; Silva-Caminha et al., 2010) and the foraminifera material was compared with descriptions published in classic works (e. g., Ellis and Messina, 1940 et. seq.; Loeblich and Tappan, 1957, 1988; Kennett and Srinivasan, 1983; Bolli et al., 1985; Morkhoven et al., 1986; Bolli et al., 1994). The chronostratigraphic interpretation of the palynological material is based on the palynological zonation proposed by Jaramillo et al. (2011) for northern South America and the interpretation for the micropaleontological material is based on the zonation scheme proposed by Blow (1969) and Berggren et al. (1995).

### 3.4. P-wave residuals

We used an analysis of travel time residuals to detect anomalies in the P-wave velocity. Such residuals are the differences between measured arrival times and computed arrival times using a standard Earth model, in this case *iasp91* (Kennett and Engdahl, 1991). Seismic events with magnitudes greater than 5.5, registered at stations of the National Seismic Network of Colombia (RSNC, Red Sismológica Nacional de Colombia) during 2008, 2009 and 2010, at epicentral distances between 30° and 90°, were used for this analysis (Fig. 2). The origin time and hypocentral location of each event were taken from the USGS/NEIC catalog. Theoretical arrival times were computed using the software 'TauP' (Crotwell et al., 1999).

A map view of absolute results of P-wave arrival time, where location and magnitude of the travel time residuals are shown for each station, can give a first idea of the presence of features beneath the area where the earthquakes are being recorded, that are causing the P-waves to travel slower or faster than they would do according to the reference model (*iasp91*). However, the magnitude and sign of the absolute residual can be due not only to anomalies near the recorders, but also near the sources. For this reason the differential travel time residuals are useful in this case. If for the same seismic event, the travel time residuals at two stations are subtracted from each other, the effects of the structure near the source can be considered negligible, and we could identify regions were the P-wave is conducted faster or slower than other areas, and these differences will be mainly a function of discrepancies in the structure of the crust and upper mantle beneath stations (Ding and Grand, 1994; Zhou et al., 1996).

**Fig. 2.** Location of seismic events used for the P-wave velocity analysis. Selected earthquakes occurred during 2008, 2009 and 2010, have a magnitude of 5.5 (Ml or Mw) or greater, and are located at epicentral distances between 30 and 90° from Bogotá, Colombia (star).

### 3.5. Whole rock geochemistry

Eight volcanic samples were analyzed by inductively coupled plasma-mass spectrometry (ICP-MS) at Acme Analytical Laboratories Ltd. in Vancouver, Canada. A 0.2 g aliquot was weighed into a graphite crucible and mixed with 1.5 g of LiBO2 flux. The crucibles were placed in an oven and heated to 1050 °C for 15 min. The molten sample was dissolved in 5% HNO3. Calibration standards and reagent blanks were added to the sample sequence. Sample solutions were aspirated into an ICP emission spectrograph (Jarrel Ash Atom Comb 975) for determining major oxides and certain trace elements (Ba, Nb, Ni, Sr, Sc, Y & Zr), while the sample solutions were aspirated into an ICP-MS (Perkins-Elmer Elan 6000) for determination of the trace elements, including rare earth elements.

Analytical results are presented in Table 2.

### 3.6. Mineral chemistry

We have also analyzed the chemical composition of pyroxene, plagioclase and olivine of 2 volcanic samples from the two main volcanic outcrops.

One sample was analyzed using a CAMECA SX-50 electron microprobe at the Department of Lunar and Planetary Sciences at the University of Arizona, USA. Analyses were performed with a beam current of 20.0 nA and an accelerating voltage of 15 kV. Counting time was 10 s for sodium and 20 s for the rest of the elements. Microprobe analytical error varies roughly between ±0.01

**Table 2**
Whole rock analytical results from the analyzed volcanic samples.

| Basalts | Puerto Escondido outcrop | | | | | | | Necoclí o. |
|---|---|---|---|---|---|---|---|---|
| | Crystalline matrix | | | Vitreous matrix | | Blocks from peperitic facies | | Crystalline matrix |
| | ML-002B | ML-002E | ML-002K | ML-002I | ML-002J | ML-002C | ML-002H | BA06-VB |
| Major elements (%) | | | | | | | | |
| $SiO_2$ | 51.68 | 50.82 | 50.31 | 50.11 | 49.75 | 47.94 | 50.02 | 51.29 |
| $Al_2O_3$ | 17.89 | 17.41 | 16.99 | 16.34 | 17.37 | 16.26 | 16.6 | 18 |
| $Fe_2O_3$ (T) | 8.8 | 9.78 | 10.58 | 11.02 | 10.54 | 8.02 | 10.77 | 8.64 |
| MgO | 3.7 | 3.48 | 3.66 | 3.7 | 4.24 | 3.48 | 3.78 | 3.2 |
| CaO | 9.37 | 9.5 | 9.55 | 9.07 | 9.22 | 11.14 | 9.27 | 9.34 |
| $Na_2O$ | 3.21 | 3.26 | 3.23 | 2.75 | 2.96 | 2.87 | 2.83 | 3.45 |
| $K_2O$ | 2.02 | 2.09 | 1.95 | 1.69 | 1.67 | 2.77 | 1.53 | 1.99 |
| $TiO_2$ | 0.73 | 0.78 | 0.78 | 0.74 | 0.74 | 0.72 | 0.74 | 0.71 |
| $P_2O_5$ | 0.48 | 0.51 | 0.5 | 0.47 | 0.51 | 0.5 | 0.49 | 0.51 |
| MnO | 0.19 | 0.18 | 0.18 | 0.19 | 0.19 | 0.35 | 0.2 | 0.16 |
| $Cr_2O_3$ | 0.009 | 0.007 | 0.008 | 0.007 | 0.005 | 0.006 | 0.006 | 0.005 |
| Sc | 29 | 28 | 29 | 27 | 25 | 26 | 27 | 25 |
| LOI | 1.6 | 1.8 | 1.9 | 3.5 | 2.4 | 5.6 | 3.4 | 2.4 |
| Total | 99.66 | 99.63 | 99.62 | 99.62 | 99.62 | 99.64 | 99.61 | 99.68 |
| Traces elements (ppm) | | | | | | | | |
| Ba | 740 | 768 | 761 | 856 | 779 | 897 | 862 | 792 |
| Co | 28 | 28.1 | 31.1 | 29.9 | 27.8 | 23 | 28.6 | 22.5 |
| Ga | 17.6 | 18.6 | 18.4 | 17.8 | 18.9 | 16.8 | 17.4 | 17.3 |
| Hf | 1.7 | 1.8 | 1.7 | 1.8 | 1.9 | 1.6 | 1.7 | 1.4 |
| Nb | 2.3 | 2.5 | 2.1 | 2.1 | 2.1 | 2.1 | 2.1 | 2.1 |
| Rb | 31.5 | 24.6 | 22.8 | 36.8 | 18.4 | 33.6 | 32.8 | 25.4 |
| Sr | 826.7 | 805.3 | 777.2 | 859.8 | 912.2 | 704.5 | 864.3 | 889.6 |
| Ta | 0.2 | 0.1 | 0.1 | 0.1 | 0.1 | 0.1 | 0.1 | 0.1 |
| Th | 1.3 | 1.3 | 1 | 1.3 | 1.3 | 1.3 | 1.3 | 1.2 |
| U | 0.7 | 0.7 | 0.5 | 0.6 | 0.5 | 0.6 | 0.6 | 0.6 |
| V | 295 | 314 | 318 | 311 | 295 | 289 | 295 | 271 |
| Zr | 61.9 | 57 | 54.8 | 55 | 56.1 | 52.9 | 55.3 | 58.5 |
| Y | 17.7 | 19.1 | 18.7 | 18.5 | 18.7 | 18.1 | 18.1 | 16.8 |
| Cu | 0.05 | 0.02 | – | – | 0.04 | 0.87 | 0.03 | 224.9 |
| Pb | 0.04 | 0.05 | 0.04 | 0.02 | 0.04 | 0.25 | 0.03 | 1.3 |
| Ni | 1.9 | 3.1 | 2.7 | 2.6 | 2 | 1.9 | 1.6 | 11.2 |
| Nb/Yb | 1.22 | 1.36 | 1.12 | 1.15 | 1.17 | 1.19 | 1.15 | 1.19 |
| Th/Yb | 0.69 | 0.71 | 0.53 | 0.71 | 0.73 | 0.73 | 0.71 | 0.68 |
| La/Yb | 4.97 | 5.43 | 5.05 | 5.11 | 5.42 | 5.25 | 4.92 | 5.42 |
| La/Nb | 4.09 | 4 | 4.52 | 4.43 | 4.62 | 4.43 | 4.29 | 4.57 |
| Th/Ta | 6.5 | 13 | 10 | 13 | 13 | 13 | 13 | 12 |
| Ce/Ce* | 0.96 | 0.89 | 0.91 | 0.92 | 0.88 | 0.92 | 0.91 | 0.95 |
| Th/La | 0.14 | 0.13 | 0.11 | 0.14 | 0.13 | 0.14 | 0.14 | 0.13 |
| Ce/Y | 1.2 | 1.1 | 1.1 | 1.1 | 1.1 | 1.1 | 1.1 | 1.3 |
| REE (ppm) | | | | | | | | |
| La | 9.4 | 10 | 9.5 | 9.3 | 9.7 | 9.3 | 9 | 9.6 |
| Ce | 21.7 | 21.7 | 21.1 | 20.8 | 20.8 | 20.6 | 20.1 | 21.7 |
| Pr | 2.95 | 3.2 | 3.09 | 3.03 | 3.1 | 2.94 | 2.95 | 2.94 |
| Nd | 14.3 | 14.6 | 14.7 | 15.2 | 14.6 | 14.3 | 13.8 | 14.4 |
| Sm | 3.46 | 3.61 | 3.59 | 3.44 | 3.34 | 3.33 | 3.44 | 3.35 |
| Eu | 1.17 | 1.14 | 1.15 | 1.11 | 1.12 | 1.05 | 1.07 | 1.11 |
| Gd | 3.71 | 3.68 | 3.78 | 3.54 | 3.63 | 3.54 | 3.48 | 3.41 |
| Tb | 0.59 | 0.61 | 0.58 | 0.58 | 0.59 | 0.59 | 0.58 | 0.56 |
| Dy | 3.33 | 3.29 | 3.42 | 3.13 | 3.18 | 3.09 | 3.25 | 3.13 |
| Ho | 0.66 | 0.7 | 0.67 | 0.69 | 0.65 | 0.66 | 0.65 | 0.61 |
| Er | 2.06 | 1.95 | 1.96 | 1.95 | 1.89 | 1.87 | 1.87 | 1.76 |
| Tm | 0.3 | 0.29 | 0.29 | 0.28 | 0.27 | 0.27 | 0.27 | 0.26 |
| Yb | 1.89 | 1.84 | 1.88 | 1.82 | 1.79 | 1.77 | 1.83 | 1.77 |
| Lu | 0.29 | 0.28 | 0.28 | 0.27 | 0.28 | 0.27 | 0.26 | 0.26 |

and 0.04wt% (1 sigma [1$\sigma$]). Analytical results are presented in the supplementary data.

The other sample was analyzed with a JEOL/JXA86005 Superprobe at the University of Leicester, UK. Carbon coated surfaces were analyzed with an accelerating voltage of 15 kv, specimen current of 30 nA and 5–10 mm electron beam diameter. Wollastonite was used for the standardization of Si and Ca, rutile for Ti, jadeite for Al and Na, Fe304 for Fe, rhodonite for Mn, MgO for Mg, CHI4 (microcline) for K and pure Cr and Ni for Cr and Ni respectively. All the running conditions, crystals and the used standard values are described in detail by Kitsopoulos (1995) and they are available in the microprobe laboratory of Geology Department at Leicester University, UK.

Analytical results are presented in Table 3.

### 3.7. U/Pb geochronology

U–Pb detrital zircon analyses were carried out on a sample of the siliciclastic sediments (Sinú belt) associated to volcanic rocks form Puerto Escondido outcrop (Fig. 1B,C).

U–Pb geochronology was conducted at the Washington State University at Pullman following procedures established by Chang

**Table 3**
Chemical results from the analyzed minerals of the volcanic samples. PE: Puerto Escondido samples; NE: Necoclí samples.

| Sample | | | Oxides | | | | | | | | | | | Cations | | | | | | | | | | | Member | | |
|---|---|---|---|---|---|---|---|---|---|---|---|---|---|---|---|---|---|---|---|---|---|---|---|---|---|---|---|
| | | | $SiO_2$ | $TiO_2$ | $Al_2O_3$ | $Cr_2O_3$ | FeO | MnO | MgO | CaO | $Na_2O$ | $K_2O$ | Total | Si | Ti | Al | Cr | $Fe_3$ | $Fe_2$ | Mn | Mg | Ca | Na | K | Total | Ws | En | Fs |
| Piroxene | PE_1 | Core | 51.02 | 0.435 | 2.94 | 0.000 | 9.92 | 0.398 | 14.62 | 20.19 | 0.322 | 0.013 | 99.85 | 1.899 | 0.012 | 0.129 | 0.000 | 0.073 | 0.236 | 0.013 | 0.811 | 0.805 | 0.023 | – | 4.000 | 41.8 | 42.1 | 16.0 |
| | PE_2 | Rim | 50.25 | 0.417 | 3.05 | 0.015 | 10.70 | 0.358 | 14.30 | 19.86 | 0.373 | 0.011 | 99.34 | 1.883 | 0.012 | 0.135 | 0.000 | 0.102 | 0.233 | 0.011 | 0.799 | 0.797 | 0.027 | – | 4.000 | 41.3 | 41.4 | 17.4 |
| | PE_3 | Rim | 50.45 | 0.371 | 2.98 | 0.023 | 10.75 | 0.341 | 14.49 | 19.41 | 0.381 | 0.000 | 99.20 | 1.892 | 0.010 | 0.132 | 0.001 | 0.091 | 0.246 | 0.011 | 0.810 | 0.780 | 0.028 | – | 4.000 | 40.5 | 42.0 | 17.5 |
| | PE_4 | Rim | 49.27 | 0.441 | 3.76 | 0.036 | 10.24 | 0.390 | 13.77 | 19.81 | 0.362 | 0.031 | 98.11 | 1.870 | 0.013 | 0.168 | 0.001 | 0.093 | 0.232 | 0.013 | 0.779 | 0.806 | 0.027 | – | 4.000 | 42.2 | 40.8 | 17.0 |
| | PE_5 | Core | 47.84 | 0.380 | 4.87 | 0.015 | 10.20 | 0.402 | 13.45 | 19.00 | 0.378 | 0.000 | 96.53 | 1.842 | 0.011 | 0.221 | 0.000 | 0.101 | 0.227 | 0.013 | 0.772 | 0.784 | 0.028 | – | 4.000 | 41.6 | 41.0 | 17.4 |
| | PE_6 | Rim | 50.25 | 0.359 | 4.42 | 0.021 | 10.23 | 0.328 | 14.38 | 19.05 | 0.399 | 0.000 | 99.43 | 1.875 | 0.010 | 0.194 | 0.001 | 0.063 | 0.256 | 0.010 | 0.800 | 0.762 | 0.029 | – | 4.000 | 40.5 | 42.5 | 17.0 |
| | PE_7 | Core | 50.66 | 0.460 | 3.64 | 0.023 | 10.78 | 0.380 | 14.69 | 19.08 | 0.410 | 0.010 | 100.14 | 1.880 | 0.013 | 0.159 | 0.001 | 0.084 | 0.250 | 0.012 | 0.813 | 0.759 | 0.029 | – | 4.000 | 39.8 | 42.7 | 17.5 |
| | PE_8 | Rim | 45.87 | 0.428 | 6.17 | 0.000 | 9.88 | 0.384 | 13.05 | 18.89 | 0.323 | 0.006 | 95.00 | 1.792 | 0.013 | 0.284 | 0.000 | 0.131 | 0.192 | 0.013 | 0.760 | 0.791 | 0.024 | – | 4.000 | 42.2 | 40.6 | 17.2 |
| | NE_1 | Core | 50.25 | 0.439 | 2.68 | 0.042 | 10.69 | 0.37 | 14.51 | 19.62 | 0.395 | 0.002 | 99.00 | 1.888 | 0.012 | 0.119 | 0.001 | 0.107 | 0.229 | 0.012 | 0.813 | 0.790 | 0.029 | – | 4.000 | 40.7 | 41.9 | 17.3 |
| | NE_2 | Core | 46.74 | 0.139 | 5.21 | 0.022 | 15.40 | 0.497 | 11.74 | 17.40 | 0.469 | 0.027 | 97.64 | 1.809 | 0.004 | 0.238 | 0.001 | 0.171 | 0.328 | 0.016 | 0.677 | 0.721 | 0.035 | – | 4.000 | 38.0 | 35.7 | 26.3 |
| | NE_3 | Core | 47.14 | 0.129 | 5.06 | 0.021 | 15.04 | 0.427 | 11.62 | 18.28 | 0.457 | 0.015 | 98.19 | 1.814 | 0.004 | 0.230 | 0.001 | 0.169 | 0.315 | 0.014 | 0.667 | 0.754 | 0.034 | – | 4.000 | 39.6 | 35.0 | 25.4 |
| | NE_4 | Core | 47.34 | 0.125 | 5.06 | 0.007 | 14.47 | 0.404 | 12.08 | 17.89 | 0.452 | 0.021 | 97.85 | 1.823 | 0.004 | 0.230 | 0.000 | 0.151 | 0.315 | 0.013 | 0.693 | 0.738 | 0.034 | – | 4.000 | 38.9 | 36.5 | 24.6 |
| | NE_5 | Core | 46.73 | 0.164 | 5.07 | 0.053 | 15.27 | 0.440 | 11.19 | 18.53 | 0.414 | 0.018 | 97.89 | 1.809 | 0.005 | 0.231 | 0.002 | 0.172 | 0.323 | 0.014 | 0.646 | 0.768 | 0.031 | – | 4.000 | 40.3 | 33.8 | 25.9 |
| | NE_6 | Core | 47.03 | 0.154 | 4.71 | 0.025 | 14.46 | 0.438 | 11.48 | 18.37 | 0.427 | 0.019 | 97.11 | 1.830 | 0.004 | 0.216 | 0.001 | 0.147 | 0.324 | 0.014 | 0.666 | 0.766 | 0.032 | – | 4.000 | 40.3 | 35.0 | 24.7 |
| | NE_7 | Core | 46.66 | 0.129 | 5.62 | 0.003 | 13.66 | 0.393 | 11.95 | 18.92 | 0.425 | 0.028 | 97.80 | 1.794 | 0.004 | 0.255 | 0.000 | 0.182 | 0.257 | 0.013 | 0.685 | 0.779 | 0.032 | – | 4.000 | 40.9 | 36.0 | 23.1 |
| | NE_8 | Core | 46.62 | 0.126 | 4.57 | 0.000 | 15.48 | 0.495 | 11.67 | 18.03 | 0.425 | 0.059 | 97.46 | 1.811 | 0.004 | 0.209 | 0.000 | 0.194 | 0.308 | 0.016 | 0.676 | 0.750 | 0.032 | – | 4.000 | 38.9 | 35.0 | 26.1 |
| | NE_9 | Core | 46.85 | 0.147 | 4.52 | 0.004 | 16.05 | 0.444 | 10.79 | 18.43 | 0.425 | 0.041 | 97.69 | 1.824 | 0.004 | 0.207 | 0.000 | 0.168 | 0.354 | 0.015 | 0.626 | 0.769 | 0.032 | – | 4.000 | 40.1 | 32.7 | 27.2 |
| | NE_10 | Core | 46.64 | 0.150 | 5.03 | 0.013 | 14.53 | 0.431 | 11.65 | 18.66 | 0.417 | 0.000 | 97.52 | 1.805 | 0.004 | 0.229 | 0.000 | 0.184 | 0.287 | 0.014 | 0.672 | 0.773 | 0.031 | – | 4.000 | 40.4 | 35.1 | 24.5 |
| | NE_11 | Core | 46.49 | 0.145 | 4.66 | 0.040 | 14.83 | 0.431 | 11.17 | 18.76 | 0.468 | 0.021 | 97.01 | 1.813 | 0.004 | 0.214 | 0.001 | 0.185 | 0.299 | 0.014 | 0.649 | 0.784 | 0.035 | – | 4.000 | 40.9 | 33.9 | 25.2 |
| | NE_12 | Core | 47.14 | 0.142 | 4.88 | 0.000 | 15.16 | 0.000 | 11.76 | 17.92 | 0.000 | 0.000 | 97.00 | 1.841 | 0.004 | 0.225 | 0.000 | 0.084 | 0.411 | 0.000 | 0.685 | 0.750 | 0.000 | – | 4.000 | 38.9 | 35.5 | 25.7 |
| | NE_13 | Core | 46.46 | 0.113 | 5.16 | 0.004 | 14.35 | 0.447 | 11.89 | 18.29 | 0.493 | 0.021 | 97.22 | 1.799 | 0.003 | 0.236 | 0.000 | 0.196 | 0.268 | 0.015 | 0.686 | 0.759 | 0.037 | – | 4.000 | 39.7 | 35.9 | 24.3 |
| | NE_14 | Rim | 47.44 | 0.147 | 5.09 | 0.034 | 14.10 | 0.433 | 12.65 | 18.24 | 0.426 | 0.012 | 98.57 | 1.808 | 0.004 | 0.229 | 0.001 | 0.178 | 0.272 | 0.014 | 0.719 | 0.745 | 0.031 | – | 4.000 | 38.9 | 37.6 | 23.5 |
| | NE_15 | Core | 47.03 | 0.125 | 4.92 | 0.000 | 14.32 | 0.455 | 11.85 | 18.51 | 0.480 | 0.008 | 97.69 | 1.814 | 0.004 | 0.224 | 0.000 | 0.177 | 0.284 | 0.015 | 0.682 | 0.765 | 0.036 | – | 4.000 | 40.1 | 35.7 | 24.2 |
| | | | | | | | | | | | | | | | | | | | | | | | | | | An | Ab | Or |
| Plagioclase | PE_1 | Core | 52.04 | 0.00 | 28.79 | 0.002 | 1.31 | 0.029 | 0.293 | 12.21 | 4.13 | 0.529 | 99.34 | 2.000 | 0.000 | 1.304 | 0.000 | 0.877 | 0.042 | 0.001 | 0.017 | 0.503 | 0.308 | 0.026 | 5.077 | 60.1 | 36.8 | 3.1 |
| | PE_2 | Rim | 52.70 | 0.05 | 28.58 | 0.000 | 0.87 | 0.000 | 0.100 | 11.62 | 4.48 | 0.660 | 99.07 | 2.024 | 0.002 | 1.293 | 0.000 | 0.876 | 0.028 | 0.000 | 0.006 | 0.478 | 0.334 | 0.032 | 5.073 | 56.6 | 39.5 | 3.8 |
| | PE_3 | Core | 51.57 | 0.03 | 28.99 | 0.000 | 0.83 | 0.000 | 0.082 | 11.75 | 4.13 | 0.651 | 98.02 | 1.998 | 0.001 | 1.324 | 0.000 | 0.884 | 0.027 | 0.000 | 0.005 | 0.488 | 0.310 | 0.032 | 5.068 | 58.8 | 37.4 | 3.9 |
| | PE_4 | Core | 51.33 | 0.01 | 28.36 | 0.012 | 0.75 | 0.020 | 0.091 | 12.25 | 4.02 | 0.597 | 97.43 | 2.001 | 0.000 | 1.303 | 0.000 | 0.889 | 0.024 | 0.001 | 0.005 | 0.511 | 0.304 | 0.030 | 5.069 | 60.5 | 36.0 | 3.5 |
| | PE_5 | Core | 53.09 | 0.03 | 29.09 | 0.002 | 0.82 | 0.000 | 0.075 | 11.85 | 4.55 | 0.607 | 100.12 | 2.021 | 0.001 | 1.305 | 0.000 | 0.868 | 0.026 | 0.000 | 0.004 | 0.483 | 0.336 | 0.029 | 5.074 | 57.0 | 39.6 | 3.5 |
| | PE_6 | Rim | 49.19 | 0.00 | 31.60 | 0.019 | 0.75 | 0.000 | 0.075 | 14.07 | 3.18 | 0.321 | 99.20 | 1.896 | 0.000 | 1.435 | 0.001 | 0.879 | 0.024 | 0.000 | 0.004 | 0.581 | 0.238 | 0.016 | 5.073 | 69.6 | 28.5 | 1.9 |
| | PE_7 | Core | 51.82 | 0.00 | 29.35 | 0.000 | 0.84 | 0.003 | 0.090 | 12.87 | 3.98 | 0.499 | 99.45 | 1.988 | 0.000 | 1.327 | 0.000 | 0.875 | 0.027 | 0.000 | 0.005 | 0.529 | 0.296 | 0.024 | 5.071 | 62.3 | 34.8 | 2.9 |
| | PE_8 | Core | 51.97 | 0.07 | 29.37 | 0.000 | 0.82 | 0.000 | 0.097 | 11.88 | 4.26 | 0.557 | 99.02 | 1.997 | 0.002 | 1.330 | 0.000 | 0.877 | 0.026 | 0.000 | 0.006 | 0.489 | 0.317 | 0.027 | 5.071 | 58.6 | 38.1 | 3.3 |
| | PE_9 | Core | 51.77 | 0.00 | 29.31 | 0.000 | 0.97 | 0.019 | 0.146 | 11.53 | 4.27 | 0.610 | 98.62 | 1.996 | 0.000 | 1.332 | 0.000 | 0.880 | 0.031 | 0.001 | 0.008 | 0.476 | 0.319 | 0.030 | 5.073 | 57.7 | 38.6 | 3.6 |
| | PE_10 | Core | 48.05 | 0.05 | 26.43 | 0.002 | 0.98 | 0.000 | 0.130 | 10.91 | 3.79 | 0.836 | 91.17 | 1.981 | 0.001 | 1.284 | 0.000 | 0.941 | 0.034 | 0.000 | 0.008 | 0.482 | 0.303 | 0.044 | 5.078 | 58.2 | 36.5 | 5.3 |
| | PE_11 | Core | 53.05 | 0.02 | 28.27 | 0.000 | 1.18 | 0.028 | 0.174 | 10.85 | 4.60 | 0.761 | 98.93 | 2.039 | 0.001 | 1.280 | 0.000 | 0.877 | 0.038 | 0.001 | 0.010 | 0.447 | 0.343 | 0.037 | 5.072 | 54.0 | 41.5 | 4.5 |
| | PE_12 | Core | 49.83 | 0.00 | 30.32 | 0.000 | 0.78 | 0.023 | 0.092 | 11.77 | 3.97 | 0.545 | 97.33 | 1.944 | 0.000 | 1.394 | 0.000 | 0.890 | 0.025 | 0.001 | 0.005 | 0.492 | 0.300 | 0.027 | 5.078 | 60.0 | 36.7 | 3.3 |
| | PE_13 | Rim | 50.32 | 0.01 | 29.25 | 0.016 | 0.87 | 0.028 | 0.100 | 11.42 | 4.04 | 0.640 | 96.71 | 1.973 | 0.000 | 1.351 | 0.000 | 0.894 | 0.029 | 0.001 | 0.006 | 0.480 | 0.307 | 0.032 | 5.074 | 58.6 | 37.5 | 3.9 |
| | PE_14 | Rim | 49.52 | 0.02 | 28.78 | 0.000 | 0.83 | 0.006 | 0.084 | 11.93 | 3.89 | 0.597 | 95.65 | 1.962 | 0.001 | 1.344 | 0.000 | 0.904 | 0.028 | 0.000 | 0.005 | 0.506 | 0.298 | 0.030 | 5.078 | 60.6 | 35.7 | 3.6 |
| | PE_15 | Core | 52.56 | 0.03 | 29.61 | 0.000 | 0.83 | 0.000 | 0.071 | 12.48 | 4.18 | 0.550 | 100.31 | 1.999 | 0.001 | 1.327 | 0.000 | 0.868 | 0.026 | 0.000 | 0.004 | 0.509 | 0.308 | 0.027 | 5.069 | 60.3 | 36.5 | 3.2 |
| | PE_16 | Core | 51.87 | 0.00 | 29.33 | 0.045 | 0.87 | 0.033 | 0.094 | 11.16 | 4.48 | 0.726 | 98.60 | 1.999 | 0.000 | 1.333 | 0.001 | 0.880 | 0.028 | 0.001 | 0.005 | 0.461 | 0.335 | 0.036 | 5.079 | 55.4 | 40.3 | 4.3 |
| | PE_17 | Core | 51.67 | 0.04 | 29.03 | 0.006 | 0.83 | 0.051 | 0.089 | 11.06 | 4.53 | 0.768 | 98.08 | 2.001 | 0.001 | 1.325 | 0.000 | 0.884 | 0.027 | 0.002 | 0.005 | 0.459 | 0.340 | 0.038 | 5.082 | 54.8 | 40.7 | 4.5 |
| | PE_18 | Core | 48.98 | 0.03 | 28.81 | 0.039 | 1.65 | 0.044 | 0.237 | 11.70 | 3.75 | 0.503 | 95.74 | 1.945 | 0.001 | 1.348 | 0.001 | 0.906 | 0.055 | 0.001 | 0.014 | 0.498 | 0.289 | 0.025 | 5.084 | 61.3 | 35.6 | 3.1 |
| | PE_19 | Core | 49.03 | 0.04 | 28.19 | 0.035 | 0.77 | 0.007 | 0.085 | 11.49 | 4.11 | 0.617 | 94.37 | 1.964 | 0.001 | 1.331 | 0.001 | 0.914 | 0.026 | 0.000 | 0.005 | 0.493 | 0.319 | 0.032 | 5.087 | 58.4 | 37.8 | 3.7 |
| | PE_20 | Rim | 50.47 | 0.00 | 29.79 | 0.045 | 0.77 | 0.028 | 0.115 | 11.47 | 4.14 | 0.613 | 97.45 | 1.966 | 0.000 | 1.367 | 0.001 | 0.888 | 0.025 | 0.001 | 0.007 | 0.479 | 0.313 | 0.030 | 5.077 | 58.2 | 38.1 | 3.7 |
| | PE_21 | Rim | 50.06 | 0.01 | 29.93 | 0.033 | 0.87 | 0.033 | 0.096 | 11.25 | 4.24 | 0.598 | 97.11 | 1.956 | 0.000 | 1.378 | 0.001 | 0.891 | 0.028 | 0.001 | 0.006 | 0.471 | 0.321 | 0.030 | 5.084 | 57.3 | 39.1 | 3.6 |
| | NE_1 | Core | 53.27 | 0.07 | 28.78 | 0.02 | 0.88 | 0.021 | 0.096 | 11.79 | 4.21 | 0.583 | 99.72 | 2.032 | 0.002 | 1.294 | 0.001 | 0.870 | 0.028 | 0.001 | 0.005 | 0.482 | 0.311 | 0.028 | 5.054 | 58.7 | 37.9 | 3.5 |
| | NE_2 | Core | 53.15 | 0.06 | 28.57 | 0.01 | 0.92 | 0.026 | 0.090 | 11.53 | 4.22 | 0.626 | 99.21 | 2.035 | 0.002 | 1.290 | 0.000 | 0.874 | 0.029 | 0.001 | 0.005 | 0.473 | 0.313 | 0.031 | 5.053 | 57.9 | 38.3 | 3.7 |
| | NE_3 | Core | 53.53 | 0.09 | 28.92 | 0.04 | 0.81 | 0.012 | 0.113 | 11.66 | 4.52 | 0.678 | 100.37 | 2.032 | 0.003 | 1.294 | 0.001 | 0.866 | 0.026 | 0.000 | 0.006 | 0.474 | 0.333 | 0.033 | 5.068 | 56.4 | 39.6 | 3.9 |
| | NE_4 | Core | 52.37 | 0.10 | 28.96 | 0.00 | 0.71 | 0.007 | 0.075 | 12.08 | 4.14 | 0.595 | 99.04 | 2.011 | 0.003 | 1.311 | 0.000 | 0.876 | 0.023 | 0.000 | 0.004 | 0.497 | 0.308 | 0.029 | 5.062 | 59.6 | 36.9 | 3.5 |
| | | | | | | | | | | | | | | | | | | | | | | | | | | Fo | Fa | |
| Olivine | PE_1 | Core | 37.03 | 0.00 | 0.020 | 0.000 | 29.28 | 0.758 | 33.14 | 0.279 | 0.023 | 0.000 | 100.53 | 0.993 | 0.000 | 0.001 | 0.000 | 0.014 | 0.643 | 0.017 | 1.325 | 0.008 | – | – | 3.000 | 66.9 | 33.1 | – |
| | PE_2 | Rim | 34.43 | 0.00 | 1.933 | 0.014 | 26.85 | 0.672 | 30.69 | 0.313 | 0.000 | 0.000 | 94.89 | 0.976 | 0.000 | 0.065 | 0.000 | 0.000 | 0.636 | 0.016 | 1.297 | 0.010 | – | – | 3.000 | 67.1 | 32.9 | – |
| | PE_3 | Rim | 33.52 | 0.00 | 0.630 | 0.017 | 28.69 | 0.631 | 31.95 | 0.346 | 0.000 | 0.015 | 95.79 | 0.942 | 0.000 | 0.021 | 0.000 | 0.096 | 0.578 | 0.015 | 1.338 | 0.010 | – | – | 3.000 | 66.5 | 33.5 | – |
| | PE_4 | Rim | 37.40 | 0.03 | 0.133 | 0.049 | 27.82 | 0.751 | 33.79 | 0.339 | 0.022 | 0.000 | 100.33 | 1.000 | 0.001 | 0.004 | 0.001 | 0.000 | 0.622 | 0.017 | 1.346 | 0.010 | – | – | 3.000 | 68.4 | 31.6 | – |
| | PE_5 | Core | 36.10 | 0.00 | 1.566 | 0.016 | 28.86 | 0.739 | 31.43 | 0.315 | 0.000 | 0.014 | 99.03 | 0.985 | 0.000 | 0.050 | 0.000 | 0.000 | 0.659 | 0.017 | 1.279 | 0.009 | – | – | 3.000 | 66.0 | 34.0 | – |

et al. (2006). Zircon crystals were extracted from samples by traditional methods of crushing and grinding, followed by separation with a Wilfley table, heavy liquids, and a Frantz magnetic separator. Zircons were incorporated into a 1″ epoxy mount together with zircon standards. The mounts were sanded down to a depth of ~20 microns, polished, and cleaned prior to isotopic analysis. In zircons from detrital samples, the cores of the grains were analyzed to avoid complex zircon histories (Gehrels et al., 2006). Details of analytical procedures including instrumentation are discussed in Chang et al. (2006).

For the detrital samples probability plots were obtained with the ISOPLOT 3.62 (Ludwig, 2007). Representative age populations were considered when more than three grains overlap in age (Gehrels et al., 2006). This statistical assumption relies on the fact that individual grains may sometimes represent lead-loss trajectories.

Analytical results are presented in Table 4.

## 4. Results

### 4.1. Field and petrographic constraints

Due to low relief, continuous geological exposures in northern Colombia are relatively limited. The studied mafic volcanic rocks were identified in two main outcrops, which are regionally related to siliclastic rocks of shallow plattform and low energy deltaic environments of the upper to Middle Miocene Morrocoy-El Pantano Formation and Pajuil Formation (Fig. 1C Geotec, 1997, 1999, 2003; Guzman et al., 2004; Guzman, 2007; Gómez et al., 2007). However unpublished, mining reports suggest the existence of some quarries made of similar volcanic rocks which may be related to this volcanic province discussed here.

The volcanic outcrop in the town of Puerto Escondido (Fig. 3A–L) includes three main lithological units. Massive porphyritic basalts that cuts an intercalation of lithic greywackes, shales and mudstones and peperitic basaltic volcanic breccias. Field relations show dyke-like structures with interfingered with the sedimentary rocks, as well as superimposed normal faulting.

Within the other studied exposure, in the town of Necoclí-Antioquia, the massive volcanic body is exposed as an isolated massive rock within a small quarry (Fig. 3M–O).

The massive volcanic rocks from the two localities are moderately fractured porphyritic basalts (Fig. 3A–D and M–O). They are hypocrystalline and hypidiomorphic, with calcic plagioclase $An_{53-60}$ (30–40%), augite (12–30%) and iddingsitic olivine (5–16%) as the main phenocrysts phase that can reach up to 4.5 mm in size. The matrix is made of pale brown glass (5–15%), with prismatic microlites of plagioclase (5–20%) and augite (3–12%). Spherulites and pearlitic textures, as well as formation of paragonite in their fractures, are common features. Some phenocrysts show undulatory extinction and normal zoning. Other samples present a vitreous matrix making up approximately 40% of the volume.

The immature sandstones are intercalated with shales and mudstone (Fig. 3E–H). They are subangular and poorly sorted of middle to fine grain size (1–10 mm), and classified as conglomeratic to fine grain lithic greywackes. The matrix and cement (15–35%) include volcanic glass and carbonates, whereas the framework grains include abundant porphyritic volcanic clasts (10–20%), felsic igneous and mudstones lithics (6–16%) as well as bioclasts (2–11%). feldspars (6–26%), quartz (4–23%) and some augite and hornblende crystals (8–14%) are also common.

The peperitic basaltic volcanic breccia (Fig. 3I–L) consists of a mixture of sedimentary and igneous components which are mainly formed by fragments of 0.1–1 m monomictic basalt blocks. All these volcanic blocks are similar to the massive porphyritic basalts, these are polyhedral, sub-equant and with curviplanar surfaces. There are also some sandstone and mudstone blocks (10–50 cm long), but they are intensely fractured with corroded edges. All blocks are embedded in a fine to coarse grained matrix of poorly sorted lithic greywacke, which include glass, bioclasts and mafic to intermediate volcanic and sedimentary lithics. The mixture between curviplanar volcanic blocks and sediments, including the presence of glassy matrix in both the breccias and the sandstones, the corroded edges of the sedimentary lithics, and the presence of lithic greywacke in cracks of porphyritic basalt blocks, are similar to close-packed peperites, which suggest that magmatism and sedimentation were relatively contemporaneous (Scrope, 1858; Busby-Spera and White, 1987; White et al., 2000; Skilling et al., 2002; Wohletz, 2002). Compositionally and genetically, these facies are classified as peperitic basaltic volcanic breccia (McPhie et al., 1993).

### 4.2. Ar–Ar geochronology

Three new Ar–Ar geochronological ages were obtained on the volcanic rocks samples from northwestern Colombian. Two samples were from the Puerto Escondido outcrop and the other from the Necoclí outcrop. Summary of the obtained results are presented in Table 1 and Fig. 4.

Sample MLC-021-M2 from the massive basalts of Puerto Escondido, defined a 3-step plateau age of 13.24 ± 0.64 Ma with the age spectrum comprising 79.18% of total $^{39}Ar$ released and an associated isochron of 14.0 ± 2.0 Ma (Fig. 4A). Similarly, sample MLC-019-M5 from a basaltic block of the peperitic breccia of the Puerto Escondido outcrop, defined a plateau age of 13.43 ± 0.40 Ma in four steps with 82.84% of the released $^{39}Ar$, and an isochron age of 12.88 ± 0.67 Ma (Fig. 4B). Sample BA06-VB from the Necoclí outcrop, presents a plateau age of 14.4 ± 0.3 Ma with 50% of the released $^{39}Ar$ and an isochron age of 14.3 ± 0.15 Ma (Fig. 4C).

These ages are interpreted as related to the magmatic crystallization of the volcanic rocks to ca.13-14 Ma. The similarity in age between the basaltic block and the 2 massive basalts, and paleontological constraints for the host sediments of these volcanic rocks (Middle Miocene) confirms the peperitic-like eruption style and the contemporaneous character of the volcanic activity in the two studied outcrops.

### 4.3. Biostratigraphy

#### 4.3.1. Palynological results

Good recovery of palynomorphs with more than 200 individuals was observed in the sample MLC-018M2. Spores of the genus *Psilatriletes* and specimens of *Laevigatosporites tibuensis* and *Polypodiisporites* spp dominate the palynoflora. It is also common to find specimens of *Psilatriletes peruanus*, *Crassoretitriletes vanraadshooveni*, *Magnastriatites grandiosus* and *Foveotriletes ornatus*, among others. A few specimens of angiosperm pollen were found including *Mauritiidites franciscoi var. minutus*, *Clavainaperturites microclavatus* and *Proteacidites triangulatus* among others.

The palynological recovery in the sample MLC-019M7 was very low with only few specimens of Mauritiidites franciscoi var. minutus, Polypodiisporites sp., Retitriletes sommeri and Verrucatosporites usmensis.

The palynological association, found especially in the sample MLC 018M2, can be related to the palynological zone T-15 (Jaramillo et al., 2011), which is dated as Middle Miocene (~12.7–14.2 ma).

#### 4.3.2. Foraminiferal results

The recovery of foraminiferal tests in five samples was moderate to very low ranging from 150 to 5 specimens of both planktonic and

**Table 4**
U–Pb detrital zircon analytical results of host sandstones (Sinú belt) from Puerto Escondido outcrop.

| Sample | $^{207}Pb$ | 1 Sigma | $^{206}Pb$ | 1 Sigma | Error | $^{238}U$ | 1 Sigma | $^{207}Pb$ | 1 Sigma | $^{206}/^{238}$ | 1 Sigma | $^{207}/^{206}$ | 1σ | Best age | 1σ |
|---|---|---|---|---|---|---|---|---|---|---|---|---|---|---|---|
| ML-002A | $^{235}U$ | % Err | $^{238}U$ | % Err | Correl. | $^{206}Pb$ | % Err | $^{206}Pb$ | % Err | Age | Abs err | Age | Abs err | Ma | Abs (Ma) |
| | Use these columns for Wetherill Concordia | | | | | | Use these for Tera-Wasserburg concordia | | | | | | | | |
| ML-002A_60 | 0.7529 | 0.0186 | 0.0836 | 0.0015 | 0.0810 | 11.9602 | 0.0180 | 0.0653 | 0.0099 | 517.6389 | 8.9628 | 784.3128 | 20.5974 | 517.64 | 8.96 |
| ML-002A_59 | 1.8188 | 0.0455 | 0.1799 | 0.0032 | 0.0709 | 5.5587 | 0.0180 | 0.0733 | 0.0105 | 1066.4247 | 17.6189 | 1022.9930 | 21.0247 | 1022.99 | 21.02 |
| ML-002A_58 | 2.3118 | 0.0594 | 0.1985 | 0.0038 | 0.0639 | 5.0366 | 0.0191 | 0.0844 | 0.0102 | 1167.5059 | 20.4023 | 1302.8784 | 19.6087 | 1302.88 | 19.61 |
| ML-002A_57 | 2.1794 | 0.0597 | 0.2011 | 0.0041 | 0.0681 | 4.9725 | 0.0202 | 0.0786 | 0.0116 | 1181.2552 | 21.7841 | 1162.0500 | 22.7705 | 1162.05 | 22.77 |
| ML-002A_56 | 0.0639 | 0.0022 | 0.0101 | 0.0002 | 0.0947 | 99.4777 | 0.0210 | 0.0461 | 0.0203 | 64.4791 | 1.3478 | 1.4726 | 48.2833 | 64.48 | 1.35 |
| ML-002A_55 | 0.0830 | 0.0025 | 0.0129 | 0.0003 | 0.0997 | 77.7129 | 0.0197 | 0.0468 | 0.0163 | 82.4225 | 1.6111 | 39.1465 | 38.5642 | 82.42 | 1.61 |
| ML-002A_54 | 2.1409 | 0.0634 | 0.2015 | 0.0043 | 0.0686 | 4.9624 | 0.0216 | 0.0771 | 0.0134 | 1183.4492 | 23.2768 | 1122.5419 | 26.3936 | 1122.54 | 26.39 |
| ML-002A_53 | 0.0828 | 0.0028 | 0.0126 | 0.0003 | 0.0896 | 79.1247 | 0.0201 | 0.0475 | 0.0202 | 80.9611 | 1.6203 | 76.1668 | 47.3103 | 80.96 | 1.62 |
| ML-002A_52 | 0.0855 | 0.0029 | 0.0121 | 0.0003 | 0.0924 | 82.5185 | 0.0218 | 0.0512 | 0.0180 | 77.6513 | 1.6807 | 249.5951 | 40.9761 | 77.65 | 1.68 |
| ML-002A_51 | 0.0982 | 0.0037 | 0.0131 | 0.0003 | 0.0827 | 76.1037 | 0.0234 | 0.0542 | 0.0220 | 84.1539 | 1.9584 | 379.9204 | 48.7382 | 84.15 | 1.96 |
| ML-002A_50 | 0.0971 | 0.0031 | 0.0148 | 0.0003 | 0.0976 | 67.6803 | 0.0204 | 0.0476 | 0.0172 | 94.5512 | 1.9142 | 81.8042 | 40.3959 | 94.55 | 1.91 |
| ML-002A_49 | 0.2710 | 0.0072 | 0.0386 | 0.0007 | 0.1026 | 25.9068 | 0.0192 | 0.0509 | 0.0116 | 244.1486 | 4.6048 | 237.3909 | 26.4646 | 244.15 | 4.60 |
| ML-002A_48 | 2.5455 | 0.0630 | 0.2204 | 0.0039 | 0.0626 | 4.5367 | 0.0179 | 0.0838 | 0.0101 | 1284.1255 | 20.8038 | 1286.8342 | 19.5153 | 1286.83 | 19.52 |
| ML-002A_47 | 0.0958 | 0.0031 | 0.0132 | 0.0003 | 0.0856 | 75.9494 | 0.0201 | 0.0528 | 0.0179 | 84.3238 | 1.6800 | 318.9757 | 40.2887 | 84.32 | 1.68 |
| ML-002A_46 | 0.5379 | 0.0139 | 0.0688 | 0.0013 | 0.0907 | 14.5308 | 0.0184 | 0.0567 | 0.0113 | 429.0397 | 7.6167 | 479.2178 | 24.8179 | 429.04 | 7.62 |
| ML-002A_45 | 0.3865 | 0.0107 | 0.0435 | 0.0008 | 0.0773 | 23.0009 | 0.0190 | 0.0645 | 0.0146 | 274.3463 | 5.0914 | 757.2623 | 30.5836 | 274.35 | 5.09 |
| ML-002A_44 | 3.6017 | 0.0809 | 0.2728 | 0.0050 | 0.0623 | 3.6662 | 0.0185 | 0.0958 | 0.0078 | 1554.8205 | 25.4649 | 1543.2436 | 14.6250 | 1543.24 | 14.63 |
| ML-002A_43 | 2.9309 | 0.0691 | 0.2408 | 0.0046 | 0.0661 | 4.1533 | 0.0190 | 0.0883 | 0.0091 | 1390.7260 | 23.6831 | 1388.7223 | 17.2934 | 1388.72 | 17.29 |
| ML-002A_42 | 3.4509 | 0.0784 | 0.2649 | 0.0049 | 0.0623 | 3.7746 | 0.0184 | 0.0945 | 0.0084 | 1515.0105 | 24.8185 | 1517.5813 | 15.6694 | 1517.58 | 15.67 |
| ML-002A_41 | 3.4501 | 0.0767 | 0.2662 | 0.0049 | 0.0638 | 3.7567 | 0.0184 | 0.0940 | 0.0075 | 1521.4505 | 24.8789 | 1508.1513 | 14.1454 | 1508.15 | 14.15 |
| ML-002A_40 | 0.3458 | 0.0099 | 0.0413 | 0.0008 | 0.0842 | 24.1871 | 0.0201 | 0.0607 | 0.0148 | 261.1609 | 5.1423 | 626.9881 | 31.6729 | 261.16 | 5.14 |
| ML-002A_39 | 0.0462 | 0.0017 | 0.0069 | 0.0002 | 0.0911 | 144.8788 | 0.0224 | 0.0486 | 0.0223 | 44.3424 | 0.9886 | 128.0642 | 51.6226 | 44.34 | 0.99 |
| ML-002A_38 | 0.0779 | 0.0022 | 0.0118 | 0.0002 | 0.1012 | 84.4413 | 0.0187 | 0.0477 | 0.0155 | 75.8934 | 1.4145 | 85.5582 | 36.3175 | 75.89 | 1.41 |
| ML-002A_37 | 0.3294 | 0.0089 | 0.0357 | 0.0007 | 0.0755 | 27.9873 | 0.0188 | 0.0669 | 0.0141 | 226.3144 | 4.1817 | 833.4016 | 29.0903 | 226.31 | 4.18 |
| ML-002A_36 | 5.3252 | 0.1200 | 0.3340 | 0.0062 | 0.0516 | 2.9938 | 0.0185 | 0.1156 | 0.0079 | 1857.8315 | 29.8286 | 1889.7382 | 14.0976 | 1889.74 | 14.10 |
| ML-002A_35 | 3.6606 | 0.0870 | 0.2731 | 0.0052 | 0.0600 | 3.6619 | 0.0191 | 0.0972 | 0.0092 | 1556.4297 | 26.4039 | 1571.5199 | 17.1142 | 1571.52 | 17.11 |
| ML-002A_34 | 1.8105 | 0.0424 | 0.1771 | 0.0033 | 0.0783 | 5.6477 | 0.0187 | 0.0742 | 0.0091 | 1050.9139 | 18.1466 | 1045.7934 | 18.2454 | 1045.79 | 18.25 |
| ML-002A_33 | 0.2645 | 0.0061 | 0.0368 | 0.0007 | 0.1068 | 27.1447 | 0.0177 | 0.0521 | 0.0098 | 233.2134 | 4.0469 | 288.7542 | 22.3223 | 233.21 | 4.05 |
| ML-002A_32 | 0.8801 | 0.0207 | 0.1024 | 0.0019 | 0.0928 | 9.7686 | 0.0187 | 0.0624 | 0.0092 | 628.2762 | 11.2067 | 686.2064 | 19.5363 | 628.28 | 11.21 |
| ML-002A_31 | 1.8219 | 0.0415 | 0.1767 | 0.0032 | 0.0784 | 5.6607 | 0.0184 | 0.0748 | 0.0085 | 1048.6817 | 17.7696 | 1063.1598 | 16.9470 | 1063.16 | 16.95 |
| ML-002A_30 | 1.8808 | 0.0520 | 0.1841 | 0.0032 | 0.0614 | 5.4313 | 0.0174 | 0.0741 | 0.0125 | 1089.4411 | 17.3746 | 1043.9280 | 24.9543 | 1043.93 | 24.95 |
| ML-002A_29 | 1.0779 | 0.0325 | 0.1217 | 0.0023 | 0.0710 | 8.2147 | 0.0190 | 0.0642 | 0.0144 | 740.5341 | 13.2514 | 748.9127 | 30.1795 | 740.53 | 13.25 |
| ML-002A_28 | 0.2331 | 0.0071 | 0.0344 | 0.0007 | 0.0990 | 29.0608 | 0.0204 | 0.0491 | 0.0135 | 218.0939 | 4.3759 | 153.9650 | 31.3684 | 218.09 | 4.38 |
| ML-002A_27 | 6.4104 | 0.1717 | 0.3713 | 0.0062 | 0.0363 | 2.6936 | 0.0168 | 0.1252 | 0.0118 | 2035.3113 | 29.2235 | 2032.1420 | 20.6685 | 2032.14 | 20.67 |
| ML-002A_26 | 1.9120 | 0.0526 | 0.1827 | 0.0032 | 0.0612 | 5.4747 | 0.0176 | 0.0759 | 0.0120 | 1081.4844 | 17.5127 | 1093.0514 | 23.9179 | 1093.05 | 23.92 |
| ML-002A_25 | 0.9823 | 0.0306 | 0.1127 | 0.0021 | 0.0701 | 8.8712 | 0.0190 | 0.0632 | 0.0156 | 688.5493 | 12.4188 | 715.2118 | 32.8327 | 688.55 | 12.42 |
| ML-002A_24 | 0.2933 | 0.0095 | 0.0400 | 0.0007 | 0.0768 | 25.0000 | 0.0183 | 0.0532 | 0.0177 | 252.8335 | 4.5421 | 336.7964 | 39.6562 | 252.83 | 4.54 |
| ML-002A_23 | 0.0958 | 0.0029 | 0.0144 | 0.0003 | 0.0938 | 69.3474 | 0.0191 | 0.0482 | 0.0149 | 92.2945 | 1.7492 | 108.6904 | 34.8867 | 92.29 | 1.75 |
| ML-002A_22 | 0.0920 | 0.0035 | 0.0139 | 0.0003 | 0.0824 | 71.8552 | 0.0205 | 0.0479 | 0.0220 | 89.0954 | 1.8180 | 95.4133 | 51.2490 | 89.10 | 1.82 |
| ML-002A_21 | 2.0896 | 0.0592 | 0.1921 | 0.0035 | 0.0584 | 5.2044 | 0.0180 | 0.0789 | 0.0128 | 1132.9881 | 18.6848 | 1169.0733 | 25.1960 | 1169.07 | 25.20 |
| ML-002A_20 | 0.3088 | 0.0091 | 0.0431 | 0.0008 | 0.0847 | 23.2267 | 0.0178 | 0.0520 | 0.0143 | 271.7342 | 4.7433 | 286.3384 | 32.3911 | 271.73 | 4.74 |
| ML-002A_19 | 0.5882 | 0.0171 | 0.0749 | 0.0014 | 0.0800 | 13.3596 | 0.0183 | 0.0570 | 0.0136 | 465.3258 | 8.2032 | 491.1955 | 29.7306 | 465.33 | 8.20 |
| ML-002A_18 | 2.3698 | 0.0675 | 0.2091 | 0.0040 | 0.0593 | 4.7814 | 0.0191 | 0.0822 | 0.0120 | 1224.2585 | 21.2940 | 1249.8983 | 23.2912 | 1249.90 | 23.29 |
| ML-002A_17 | 2.9112 | 0.0824 | 0.2400 | 0.0044 | 0.0537 | 4.1664 | 0.0184 | 0.0880 | 0.0124 | 1386.7740 | 22.9562 | 1381.9047 | 23.6221 | 1381.90 | 23.62 |
| ML-002A_16 | 0.1036 | 0.0040 | 0.0144 | 0.0003 | 0.0783 | 69.3442 | 0.0218 | 0.0521 | 0.0216 | 92.2986 | 1.9994 | 291.2608 | 48.7047 | 92.30 | 2.00 |
| ML-002A_15 | 6.4480 | 0.1891 | 0.3775 | 0.0071 | 0.0374 | 2.6489 | 0.0187 | 0.1239 | 0.0126 | 2064.6516 | 33.0106 | 2013.3779 | 22.1894 | 2013.38 | 22.19 |
| ML-002A_14 | 0.0823 | 0.0038 | 0.0130 | 0.0003 | 0.0793 | 76.7932 | 0.0233 | 0.0458 | 0.0286 | 83.4032 | 1.9275 | 0.0000 | 56.2334 | 83.40 | 1.93 |
| ML-002A_13 | 5.6165 | 0.1617 | 0.3462 | 0.0062 | 0.0382 | 2.8882 | 0.0178 | 0.1177 | 0.0126 | 1916.5798 | 29.5208 | 1921.4185 | 22.4852 | 1921.42 | 22.49 |

| | | | | | | | | | | | | | | | |
|---|---|---|---|---|---|---|---|---|---|---|---|---|---|---|---|
| ML-002A_12 | 0.0705 | 0.0023 | 0.0108 | 0.0002 | 0.0907 | 92.5154 | 0.0189 | 0.0473 | 0.0159 | 69.3055 | 1.3048 | 64.9602 | 37.3716 | 69.31 | 1.30 |
| ML-002A_11 | 1.2508 | 0.0361 | 0.1367 | 0.0024 | 0.0665 | 7.3160 | 0.0176 | 0.0664 | 0.0130 | 825.9039 | 13.6126 | 818.5982 | 26.9166 | 825.90 | 13.61 |
| ML-002A_10 | 1.8683 | 0.0581 | 0.1780 | 0.0034 | 0.0586 | 5.6173 | 0.0191 | 0.0761 | 0.0146 | 1056.1545 | 18.6108 | 1098.7294 | 28.9712 | 1098.73 | 28.97 |
| ML-002A_9 | 0.5014 | 0.0175 | 0.0567 | 0.0014 | 0.0813 | 17.6494 | 0.0251 | 0.0642 | 0.0142 | 355.2757 | 8.6542 | 748.3485 | 29.7192 | 355.28 | 8.65 |
| ML-002A_8 | 0.0756 | 0.0031 | 0.0115 | 0.0003 | 0.0820 | 86.5995 | 0.0220 | 0.0475 | 0.0239 | 74.0128 | 1.6206 | 73.7855 | 55.7558 | 74.01 | 1.62 |
| ML-002A_7 | 1.5938 | 0.0472 | 0.1607 | 0.0029 | 0.0616 | 6.2225 | 0.0181 | 0.0719 | 0.0135 | 960.7044 | 16.1306 | 984.5126 | 27.3214 | 984.51 | 27.32 |
| ML-002A_6 | 0.0435 | 0.0015 | 0.0065 | 0.0001 | 0.0822 | 153.4666 | 0.0186 | 0.0484 | 0.0183 | 41.8691 | 0.7774 | 119.6418 | 42.6303 | 41.87 | 0.78 |
| ML-002A_5 | 3.4928 | 0.1045 | 0.2686 | 0.0051 | 0.0485 | 3.7232 | 0.0189 | 0.0943 | 0.0133 | 1533.6183 | 25.7266 | 1515.0574 | 24.8412 | 1515.06 | 24.84 |
| ML-002A_4 | 0.0805 | 0.0027 | 0.0122 | 0.0002 | 0.0842 | 82.1221 | 0.0188 | 0.0480 | 0.0180 | 78.0238 | 1.4552 | 97.9646 | 42.0206 | 78.02 | 1.46 |
| ML-002A_3 | 1.1628 | 0.0351 | 0.1249 | 0.0025 | 0.0706 | 8.0044 | 0.0198 | 0.0675 | 0.0128 | 758.8873 | 14.1933 | 854.0462 | 26.3847 | 758.89 | 14.19 |
| ML-002A_2 | 0.0675 | 0.0032 | 0.0092 | 0.0002 | 0.0631 | 108.1196 | 0.0215 | 0.0529 | 0.0298 | 59.3490 | 1.2727 | 326.0217 | 66.1809 | 59.35 | 1.27 |
| ML-002A_1 | 1.9101 | 0.0565 | 0.1865 | 0.0034 | 0.0598 | 5.3611 | 0.0181 | 0.0743 | 0.0135 | 1102.5468 | 18.3254 | 1049.4565 | 26.9310 | 1049.46 | 26.93 |

benthic forms. Sample MLC-018M2 was barren of foraminifera. The preservation of most tests was regular to poor.

Sample CCR-04 showed moderate recovery of foraminifera dominated by benthic forms such as Uvigerina sp., Uvigerina isidroensis, Uvigerina cf. Uvigerina rustica, Uvigerina cf. Uvigerina ecuadorensis, Planulina sp., Sphaeroidina bulloides, Sphaeroidina sp., Melonis affinis, Melonis sp., Pullenia cf. Pullenia bulloides, Bulimina mexicana, Siphogenerina sp., Bolivina cf. Bolivina alazanensis, Nodosaria longiscata (fragments), Gyroidina cf. Gyrodina soldanii, Cibicidoides spp., Oridorsalis sp., Nodosariidae indet. (fragments), Globocassidulina ? sp. and Lenticulina sp. Among the planktonic forms were found a few specimens of Globorotalia peripheroronda, Globorotalia cf. Globorotalia peripheroronda, Globorotalia mayeri, Globorotalia cf. Globorotalia mayeri, Globorotalia cf. Globorotalia archeomenardii, Globigerinoides cf. Globigerinoides rubra, Globigerinoides cf. Globigerinoides immatura, Globigerinoides indet., Globigerina sp. and Globigerinacea indet.

The recovery amount of sample MLC-019M7 was low and its microfaunal assemblage was mainly composed of small planktonic foraminifera ($\sim$120 μm) namely *Globorotalia peripheroronda*, *Globorotalia* cf. *Globorotalia peripheroronda*, *Globorotalia mayeri*, *Globorotalia* spp., and *Globigerina* spp. A few specimens of benthic forms such as *Bulimina* sp., *Cibicidoides* sp., *Planulina* sp. and *Textulariina* indet., were also observed.

The assemblage found in sample CCR-05 showed low recovery of foraminifera and includes a few specimens of *Textulariina* indet., *Melonis* cf. *Melonis pompilioides*, *Pullenia bulloides*, *Nodosaria longiscata* (fragments), *Nodosariidae* indet., (fragments), *Fissurina* sp., *Vasicostella* sp., *Cibicidoides* sp., *Planulina wuellerstorfi*, *Rotalidae* indet., *Globorotalia peripheroronda*, *Globorotalia* cf. *Globorotalia peripheroronda*, *Globigerina bulloides*, *Globigerinacea* indet., *Globigerina* sp., *Globorotalia* sp.

Sample CCR-06 was quite similar both in composition and recovery to CCR-05. A few specimens of *Textulariina* indet., *Oridorsalis* cf. *Oridorsalis ecuadorensis*, *Anomalina pompilioides*, *Cibicidoides* sp., *Planulina wuellerstorfi*, *Glomospirella* sp., *Gyroidina* sp., *Rotalidae* indet., *Globorotalia* cf. *Globorotalia peripheroronda*, *Globoquadrina venezuelana*, *Globorotalia* sp., were observed.

Only a very few specimens of *Bulimina* sp., *Lenticulina* sp. and *Nodosariidae* indet., were observed in sample MLC-021M1.

The occurrence in some samples (CCR-04, MLC-019M7 and CCR-05) of the marked planktonic foraminifera *Globorotalia peripheroronda* is related to the planktonic foraminiferal zones N6-N10 (Blow, 1969) indicating a Middle to Lower Miocene age (Berggren et al., 1995). The last occurrence (LO) of *G. peripheroronda* has been dated as 14 Ma (Berggren et al., 1995).

Palynological and foraminiferal results in the host sediments from the Sinu belt suggest a Middle Miocene age contemporaneous to the new volcanic ages.

### 4.4. P-wave residuals

Travel time of events shown in Fig. 2 and registered by stations of the RSNC were calculated. Fig. 5 illustrates the mean of the P-wave travel time absolute residuals at each station, where negative (positive) residuals correspond to a faster (slower) structure than predicted by the reference model. It is clear that stations north of latitude 6.5°N tend to have negative time residuals whereas stations to the south of such latitude show a predominance of positive time residuals, suggesting a major difference in the structure of the crust and/or upper mantle between these regions. Although, as it was stated above, absolute travel time residuals can contain the effects of near source anomalies, we can say that there is a real signal of the local structure because seismic rays are coming for a variety of back-azimuths and epicentral

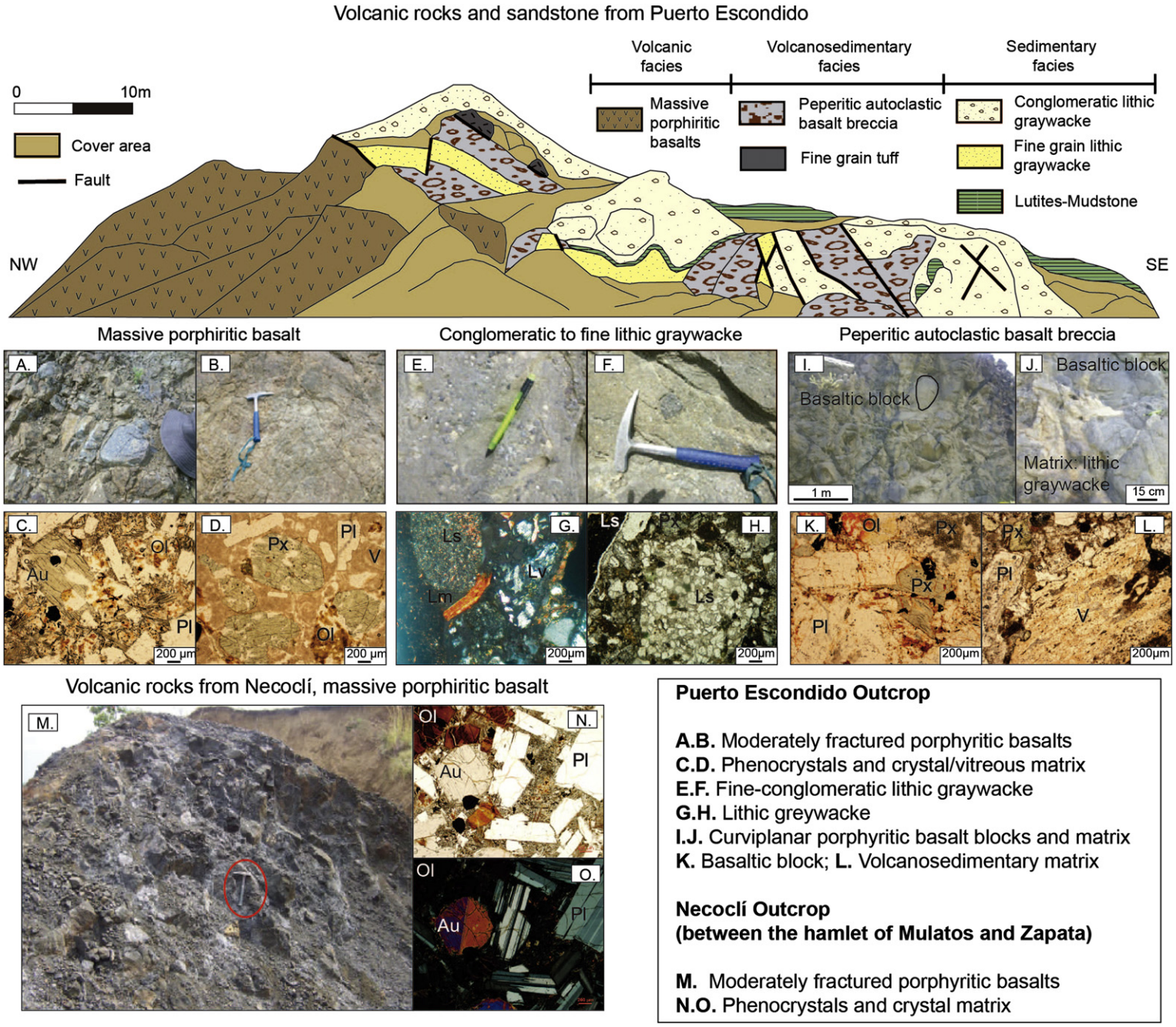


**Fig. 3.** Sketch from Puerto Escondido outcrop and view of the Necoclí outcrop (between the hamlet of Mulatos and Zapata) with images of rock samples and thin sections. Pl: Plagioclase; Px: Piroxene; Ol: Olivine; V: Vitreous matrix; Ls: Lithic sediments; Lv: Lithic volcanics; Lm: Lithic metamorphics; F: Fossil fragment.

distances so that the effects of near source structure can be considered as random and we expect them to cancel out. However, we also include results of differential time residuals that should reflect the effects of near-receiver structure only. Fig. 6 shows differential time residuals with respect to station MON; the mean (Fig. 6A) and standard deviations (Fig. 6B) of differential residuals are presented.

In general, Figs. 5 and 6 indicate that beneath the Caribbean coast and the northern Eastern Cordillera of Colombia, seismic rays have to travel through materials that have an associated P-wave velocity greater than expected from the reference model. We speculate that this could be due to the presence of a relatively cold Caribbean Slab. Stations in the Andean region and the Pacific coast tend to show positive residuals, suggesting slower P-wave velocities than for the reference models. Stations to the east of the Eastern Cordillera, which are located on the craton, show negative or less than 0.5 s residuals in Fig. 5. In Fig. 6 they tend to show smaller residuals than at station MON; when residuals at stations on the craton are larger than at MON, they do not exceed those by more than 0.5 s. However, the absolute value of the mean magnitude of the negative residuals on the craton is less than that at stations on the Caribbean coast, the northern Eastern Cordillera and the Middle-Lower Magdalena Valley (between the northern Central and Eastern Cordilleras).

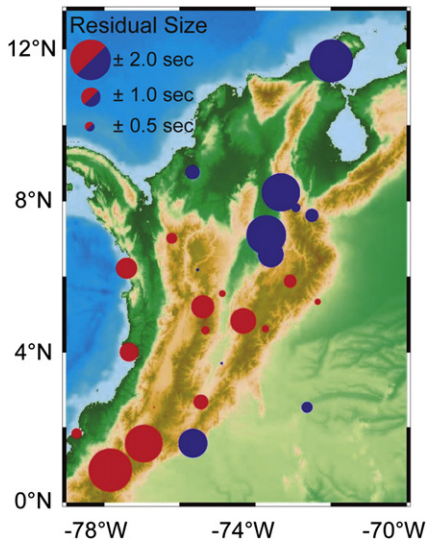


**Fig. 5.** Map view of the average absolute P-wave travel-time residual magnitude at stations of the RSNC. Circle size denotes average residual magnitude. Red (blue) colors are associated with positive (negative) residuals, corresponding to late (early) observed arrivals with respect to calculated arrival times. (For interpretation of the references to color in this figure legend, the reader is referred to the web version of this article.)

### 4.5. Whole rock geochemistry

Summary results are presented in Table 2 and Fig. 7. $SiO_2$ values for the volcanic rocks vary between 49.75% and 51.68%, with relatively high $Al_2O_3$ (15–18%), $K_2O$ (1.53–2.77%) and $Na_2O$ (2.75–4.06%) and low $TiO_2$ values (0.68–0.78%). The FeO $^{(T)}$ values range between 3.95% and 4.95%, whereas the MgO varies between 3.2% and 4.2%. The samples are classified as high $K_2O$ basalts and basaltic andesites (Fig. 7A,B; Peccerillo y Taylor, 1976; Cox et al., 1979; Hastie et al., 2007; Pearce, 1996).

Chondrite normalized patterns show some enrichment of the heavy and light rare earth elements (Fig. 7C), with La/Yb = 0.87–5.43. Cr, Ni and Zr values are low (0.52–61.56 ppm, 1.9–11.2 ppm, 35.5–61.9 ppm), whereas Ba and Sr show some moderate enrichment (740–897 ppm, 704.5–945.2 ppm). Trace elements are characterized by slight to moderate enrichment of the large-ion lithophile elements (Fig. 7D), with negative anomalies for Ta, Ti and Nb.

These chemical features are characteristic of convergent margin magmatism where fluids or melts from sediments and oceanic crust from the slab are added to the melt (Wood, 1980; Tatsumi and Eggins, 1995; Pearce, 1996; Hollings and Wyman, 2005; Haase et al., 2000; Tatsumi, 2005). This is also seen in the Ti–V ratios and the Nb/Y–Th/Yb tectonic discrimination diagrams (Fig. 7E,F; Shervais, 1982; Pearce and Peate, 1995). The high $Al_2O_3$, $NaO_2$, and

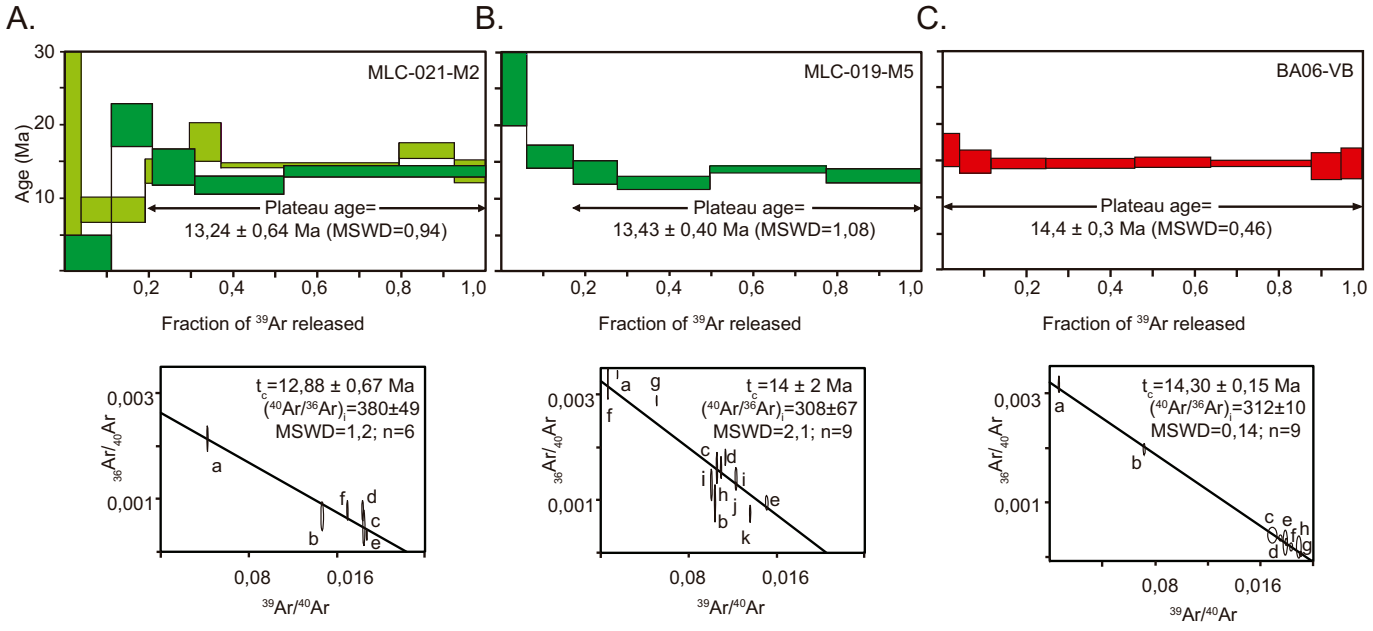


**Fig. 4.** Ar–Ar geochronology of the analyzed volcanic rocks; A. Massive volcanic rock from Puerto Escondido outcrop and B. Volcanic block of the breccia from Puerto Escondido outcrop; C. Massive volcanic rock from Necoclí (between the hamlet of Mulatos and Zapata).

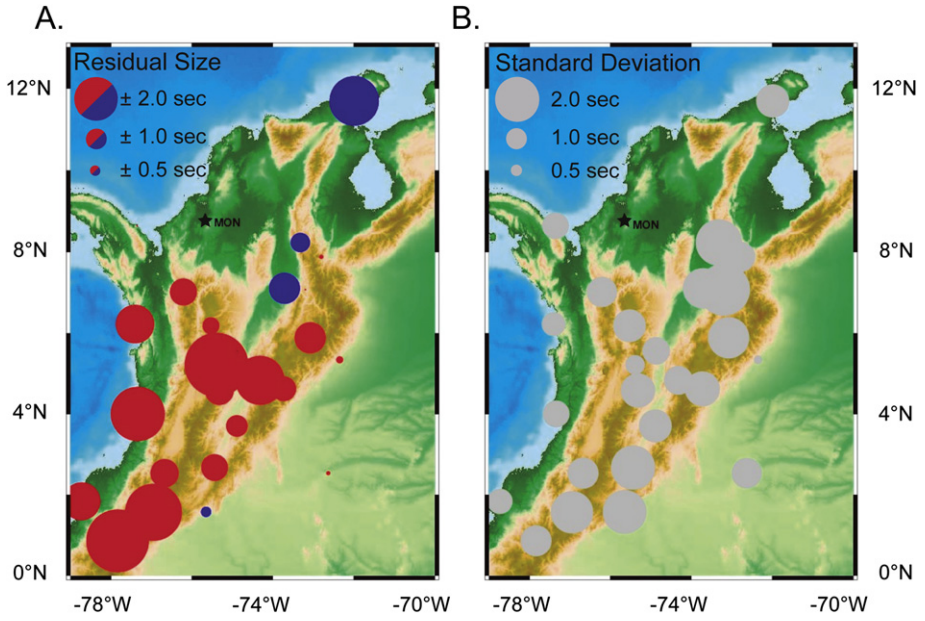


**Fig. 6.** Map view of A. average differential P-wave travel-time residual with respect to station MON, whose location is shown, and B. standard deviation of differential travel-time residuals. Sizes are proportional to magnitudes. Red (blue) colors in part A. are associated with slower (faster) local P-wave velocity structures than at station MON. (For interpretation of the references to color in this figure legend, the reader is referred to the web version of this article.)

$K_2O/Na_2O$ values (0.57–0.64), high Sr (>700 ppm), Sr/Y (>38.9), and Rb/Sr (<0.05), as well as low values of heavy REEs, Nb (<2.5 ppm), Yb (<1.9 ppm), Y (<19 ppm) are characteristic of high Al basalts formed by shallow melting of an asthenospheric mantle (Crawford et al., 1987; Niu et al., 2011).

### 4.6. Mineral chemistry

Phenocrysts and matrix clinopyroxenes have a uniform augite composition (Table 3 and Fig. 8A). Pyroxene tectonic discrimination diagrams also show that both samples are akin to convergent

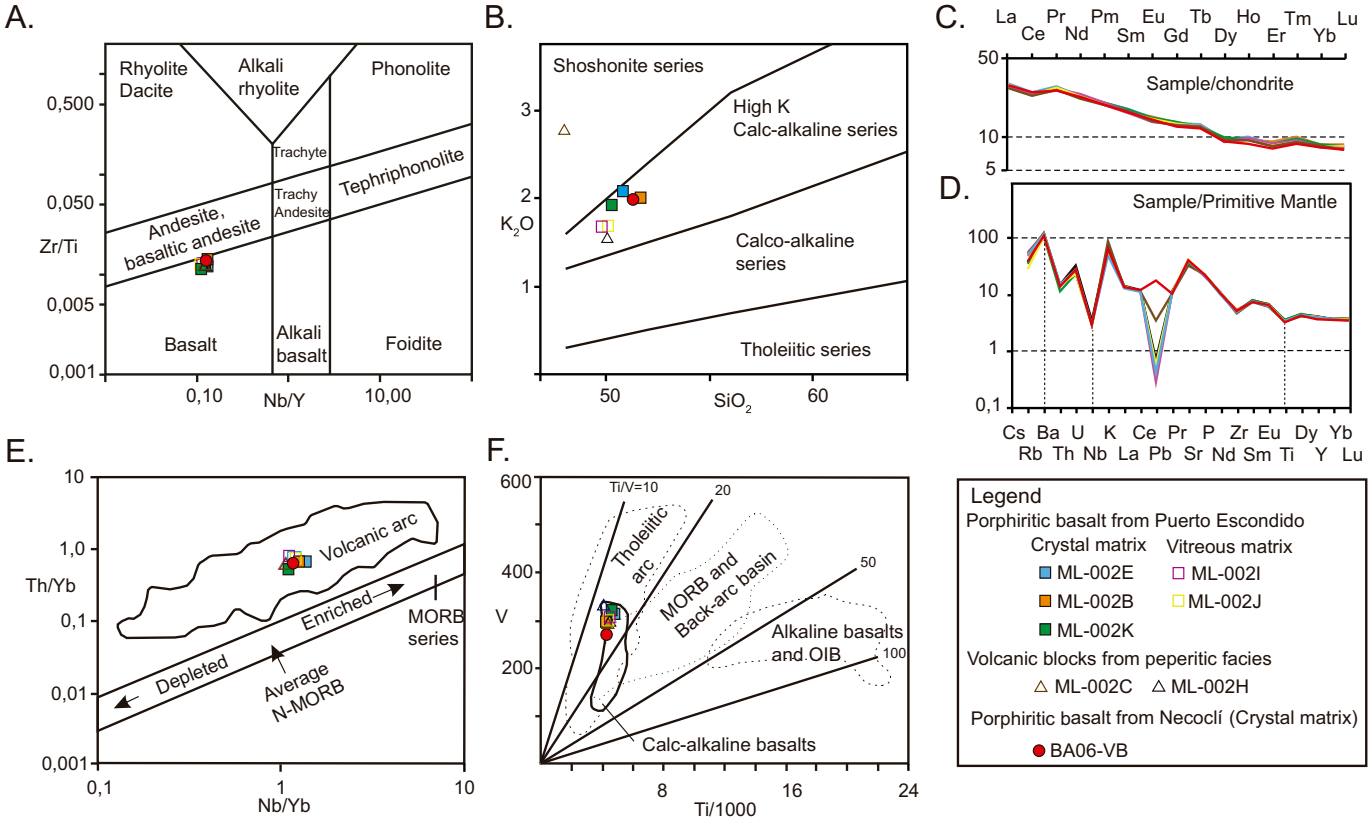


**Fig. 7.** Geochemical diagrams of the analyzed samples. A. Nb/Y vs Zr/Ti classification diagram of volcanic rocks (Pearce, 1996); B. Alkalinity series diagram after Peccerillo and Taylor (1976); C. Chondrite normalized rare earth elements plot (Nakamura, 1974); D. Primitive mantle normalized multielement diagram (Sun and McDonough, 1989); E. Nb/Yb vs Th/Yb tectonic setting discrimination diagram (Pearce and Peate, 1995). F. Ti vs V tectonic setting discrimination diagram (Shervais, 1982).

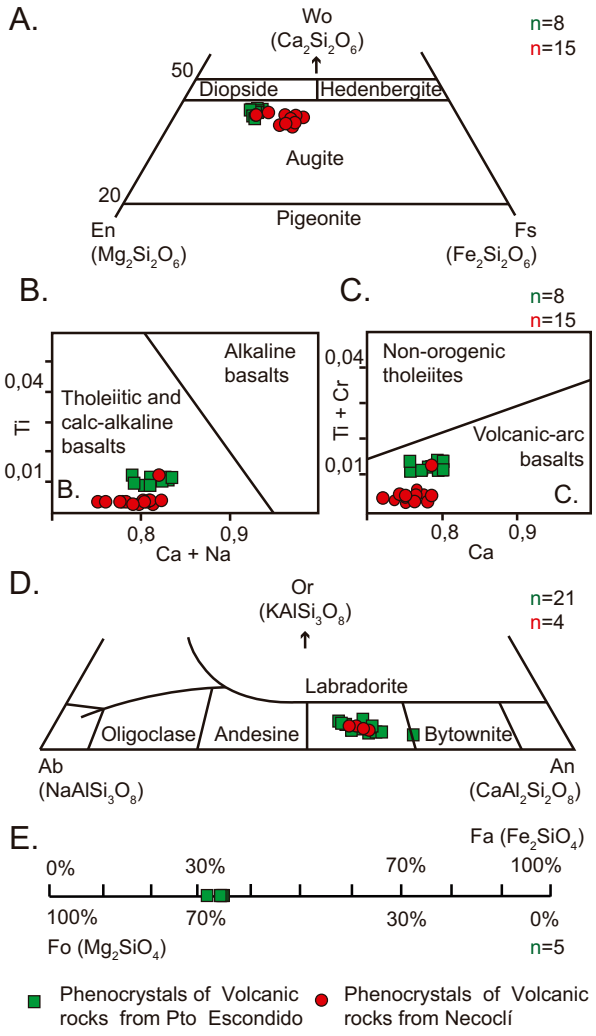


**Fig. 8.** A. Ca–Mg–Fe plot of analyzed clinopyroxenes (Morimoto et al., 1988); B.C. Pyroxenes discrimination diagrams (after Leterrier et al., 1982); D. Plagioclase discrimination diagrams; E. Olivine compositional diagrams.

margin basalts, plotting within calk-alkaline and volcanic-arc field (Fig. 8B,C; Le Bas, 1962; Leterrier et al., 1982). Plagioclase phenocrysts are mainly labradorite with compositions varying between $An_{56}$ to $An_{71}$ (Table 3 and Fig. 8D), whereas olivine shows forsteritic contents between 66% and 68% (Table 3 and Fig. 8E).

### 4.7. Heavy minerals and detrital zircon geochronology

Heavy minerals from the analyzed samples at Puerto Escondido include abundant zircon, apatite (ultrastable minerals), and abundant augite and hornblende (unstable minerals), together with epidotes and clinozoisites as well as some tourmaline and garnet crystals.

Sixty detrital zircons from a lithic greywacke from the Puerto Escondido outcrop were analyzed (Table 4 and Fig. 9). Zircons are highly concordant with main age distribution peaks including Eocene (42 Ma), Late Cretaceous (83-98 Ma), Permian (271 Ma) and Grenvillian (1036 Ma) as well as older Paleoproterozoic zircons (Fig. 9). All this ages are characteristics of the northern margin of South America, including the Central and Western Cordilleras of the Colombian Andes (Aspden et al., 1987; Spadea and Espinoza, 1996; Kerr et al., 1997; Vinasco et al., 2006; Vallejo et al., 2006; Luzieux et al., 2006; Weber et al., 2009; Cardona-Molina et al., 2006; Cardona et al., 2010; Ibañez-Mejía et al., 2010; Villagómez et al., 2011).

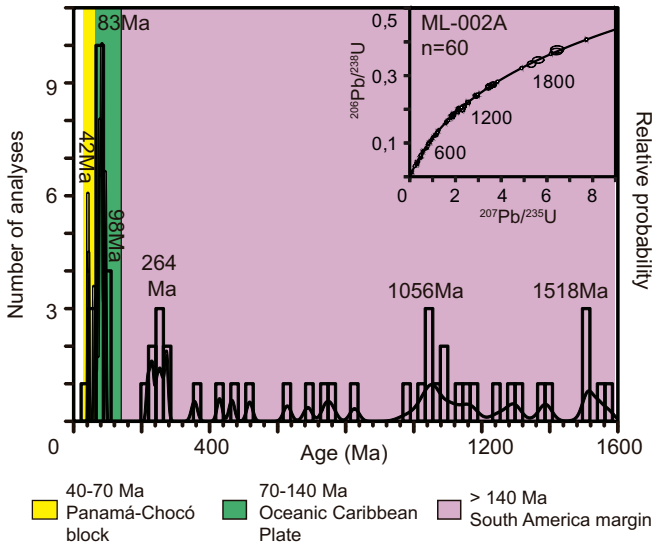


**Fig. 9.** Detrital zircon analyses of host sandstones (Sinú belt) from Puerto Escondido outcrop.

## 5. Tectonic discussion

Field relations, geochemical, geochronological and biostratigraphic data record the presence of a Middle Miocene (13-14 Ma) mafic volcanism in northernmost Colombia that intrudes platform sediments deposited over the South American plate. This volcanism intrudes and covers contemporaneous platform to deltaic sediments. The presence of detrital zircon populations older than ca. 41 Ma including Triassic and Precambrian zircons suggest that the sediments that host this magmatism were deposited within the South American margin when the Panama Block and the continental margin were already juxtaposed (Farris et al., 2011; Montes et al., 2012a,b).

Results of P-wave travel time residual analysis (Figs. 5 and 6) are consistent with the presence of a shallowly subducting Caribbean Slab, with a SE subduction direction. The prevalent negative time residuals in northern Colombia indicate a faster P-wave velocity in the near-receiver structure, where negative (blue) residuals correspond to faster structures, suggesting a cold mantle due to absence of an asthenospheric wedge. According to the anomalies in the P-wave velocities, the slab could be extending to locations to the SE of the Sinú area, beneath the Middle-Lower Magdalena Valley and the Northern Eastern Cordillera of Colombia, as suggested from the easternmost stations with mean residuals in blue in Figs. 5 and 6.

Published tomographic, seismicity and focal mechanisms analyses also suggest that a Caribbean oceanic plate is subducting under the South American continent in the Southern Caribbean including northern Colombia (Van Der Hilst and Mann, 1994; Cortes and Angelier, 2005; Corredor, 2003; Miller et al., 2009; Londoño et al., 2010; Bezada et al., 2010).

GPS measurements (Perez et al., 2001; Trenkamp et al., 2002; Weber et al., 2001) together with the analysis of motion of the Americas relative to the Atlantic-Indian hotspot reference frame (Müller et al., 1999) suggest that the Caribbean plate has been obliquely and slowly converging since the Miocene against the South American plate at a rate of 2.1 mm/y. All these geophysical constraints also suggest that current subduction of the Caribbean plate occurs at a very shallow subduction angle of 12°–19°. Such a

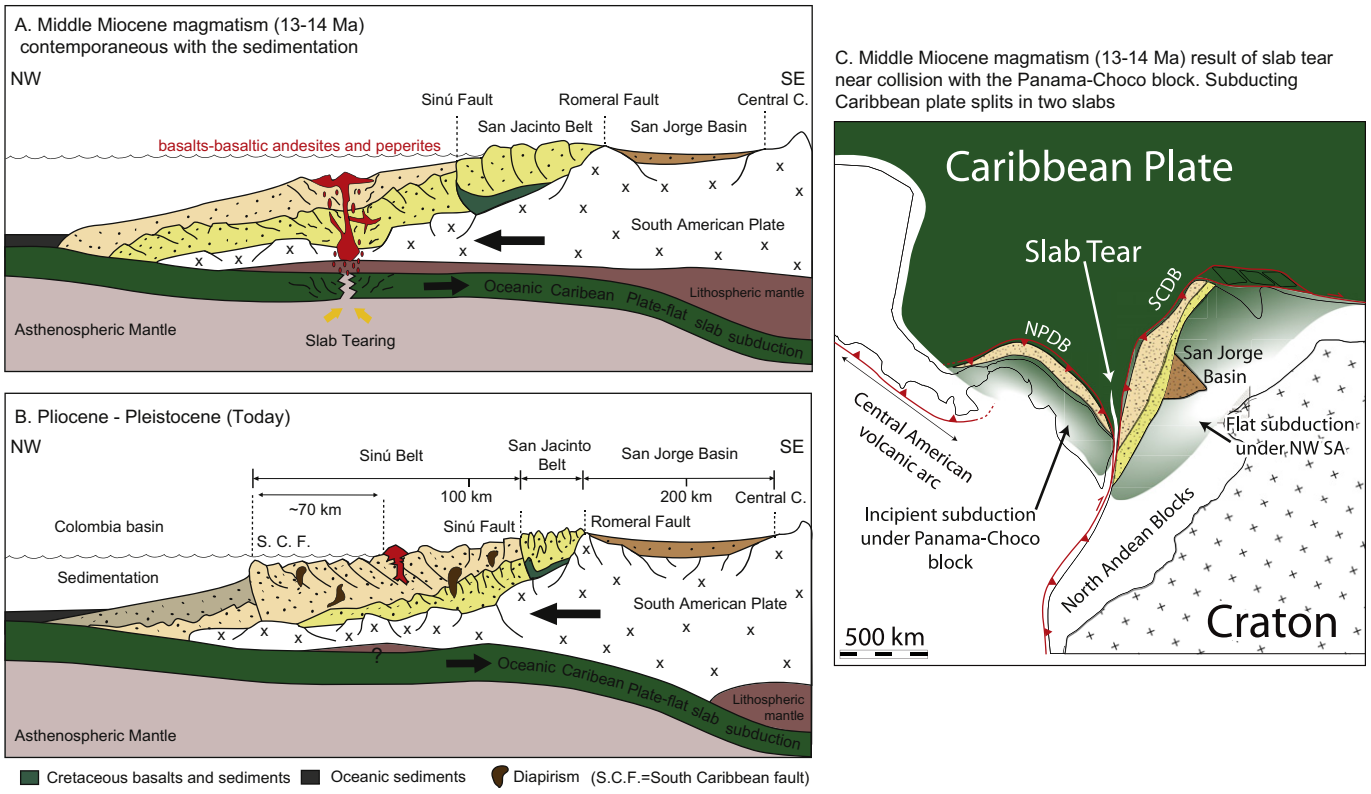


**Fig. 10.** Tectonic evolution of the volcanic rocks from Sinú belt; A. Filling and formation of Sinú-San Jacinto belts and vertical slab tear formation in the Caribbean plate: Middle Miocene magmatic event contemporary with the sedimentation from Sinú belt; B. Final uplift of Sinú-San Jacinto belts: Current framework of the margin and of the exposures of volcanic rocks. C. Map-view reconstruction during the middle Miocene magmatic event. Caribbean plate splits in two slabs dipping in different directions causing northward propagation of a slab from the collision point between the Panama-Choco block and northwestern South America. Paleogeographic configuration after Montes et al. (2012a) and Montes et al. (2012b). NPDB: north Panama deformed belt, SCDB: Southern Caribbean deformed belt.

peculiar flat slab convergence suggest that the mantle wedge along several hundreds of kilometers of the South American continental margin is not present.

The absence of a typical arc system linked to the existence of a mantle wedge and its outboard position relatively close to the trench has been commonly explained by at least three main different tectonic scenarios: (1) Ridge Subduction, (2) lower plate flexure before arriving to the trench, and (3) lithospheric scale extension associated to slab pull (Thorkelson, 1996; Hirano et al., 2006; Madsen et al., 2006; Gasparon et al., 2009; Wortel et al., 2009; Yamamoto and Hoang, 2009; Davis et al., 2010).

Model (1) is not plausible as the Caribbean plate does not include any active spreading ridge system (Mauffret and Leroy, 1997; Pindell and Kennan, 2009). Due to the very low subduction angle of the Caribbean plate, a flexure of the oceanic lithosphere as it descends (model 2) is not appropriate (Schoonmaker et al., 2005). Lithosphere scale extension (3) due to slab pull seems to be also limited as slab pull is not significant in the proximal segments of the flat slab settings (Martinod et al., 2010).

We suggest an alternative scenario where fracturing of the oceanic plate can be caused by splitting of the Caribbean plate in two slab: one under the Panama block forming the North Panama Deformed Belt, which is an active accretionary prism since the Middle Miocene (Bowland, 1984; Kellog and Vega, 1995), with a normal Wadati-Benioff zone dipping to the southwest at a normal angle (Camacho et al., 2010). In the other the slab subducts to the southeast at a very low angle under the South American continental plate (Fig. 10). This tectonic condition immediately followed the middle Miocene collision of the Panama-Choco block (Farris et al., 2011; Montes et al., 2012a,b) and the increase in the convergence rates between the North and South America in the Miocene. The contrasting dips and convergence rates of the slab (normal vs. flat) created a north-propagating tear in the subducting plate (Fig. 10) that promoted adiabatic shallow melting of the oceanic asthenospheric mantle, forming relatively high alumina and low Ti basalts with more enriched LREE and flatter HREE patterns (Niu et al., 2011). The geothermal perturbation due to asthenospheric flow during fracturing may have also promoted partial melting of thinned lithosphere in the upper plate and sediments from the oceanic crust, which is reflected in the relative fractionation of Nb from Th and Ce, which are commonly transferred from the melting of the slab and associated sediments (Zhao et al., 1993; Pearce, 1996).

## Acknowledgments

We thank the “Asociación Colombiana de Geólogos y Geofísicos del Petróleo” (ACGGP), Colciencias “Jóvenes Investigadores e innovadores – convocatoria 525, 2011” program and the “Fundación para la promoción de la Ciencia y la Tecnología del Banco de la República de Colombia” (Project 2570) for their financial support. J. Vanegas is kindly acknowledged for her help and discussion during fieldwork. G. Cañizales is also acknowledged for his help with sample preparation. We also thank Mauricio Ibañez and Jhon Cerón for providing a sample from the Necoclí outcrop (between the hamlet of Mulatos and Zapata). Many thanks to Esteban Poveda from “Servicio Geológico Colombiano” and the “Red Sismológica Nacional de Colombia” (RSNC) for generously gathering and providing the data for the P-wave analysis. The help of Rob Wilson with the microprobe at University of Leicester is greatly appreciated. We are thankful to the anonymous reviewers and J. Kellogg for

their comments and suggestions that allowed us to improve and clarify the manuscript.

## References


Aspden, J.A., McCourt, W.J., Brook, M., 1987. Geometrical control of subduction related magmatism: the Mesozoic and Cenozoic plutonic history of western Colombia. Geological Society of London 144, 893–905.

Berggren, W.A., Kent, D.V., Swisher, C.C., Aubry, M.P., 1995. A revised Cenozoic geochronology and chronostratigraphy. In: Berggren, W.A., Kent, D.V., Aubry, M.P., Hardenbol, J. (Eds.), Geochronology, Time Scales and Stratigraphic Correlation, vol. 54. SEPM Special Publication, pp. 129–212.

Bernal, R., Mann, P., Escalona, A., 2012. Defining the geometry of the subducting Caribbean slab beneath northwestern Colombia and its controls on the overriding Lower Magdalena forearc basin. In: XI Bolivarian Symposium conference, Petroleum Exploration in SubAndean Basins, Memoir 129. In Cartagena, Colombia.

Bezada, M.J., Levander, A., Schmandt, B., 2010. Subduction in the southern Caribbean: Images from finite-frequency P wave tomography. Journal of Geophysical Research 115 (B12333), 19. http://dx.doi.org/10.1029/2010JB007682.

Blow, W.H., 1969. Late Middle Eocene to Recent planktonic foraminiferal biostratigraphy. In: BrÖnnimann, P., Renz, H.H. (Eds.), Proceedings of the First International Conference on Planktonic Microfossils, Geneva, 1967. 2. Vols, vol. 1. E.J. Brill, Leiden, pp. 199–421.

Bolli, H., Saunders, J.B., 1985. Oligocene to Holocene low latitude plaktic foraminifera. In: Bolli, H.M., Saunders, J.B., Perch-Nielsen, K. (Eds.), Plankton Stratigraphy. Cambridge Earth Science Series, pp. 155–262.

Bolli, H.M., Beckmann, J.P., Saunders, J.B., 1994. Benthic Foraminiferal Biostratigraphy of the South Caribbean Region. Cambridge University Press, London, 408 p.

Bowland, C. L., 1984. Seismic Stratigraphy and Structure of Western Colombian Basin, Caribbean Sea, M.S. thesis. Austin, University of Texas at Austin, 248pp.

Burke, K., 1988. Tectonic evolution of the Caribbean. Annual Reviews on Earth and Planetary Science 16, 201–230.

Busby-Spera, C.J., White, J.D.L., 1987. Variation in peperite textures associated with differing host-sediment properties. Bullettin of Volcanology 49, 765–775.

Camacho, E., Hutton, W., Pacheco, J.F., 2010. A new look at evidence for a Wadati-Benioff zone and active convergence at the north Panama deformed belt. Bulletin of the Seismological Society of America 100 (1), 343–348.

Cardona, A., Valencia, V., Bustamante, C., García–Casco, A., Ojeda, G., Ruiz, J., Saldarriaga, M., Weber, M., 2010. Tectonomagmatic setting and provenance of the Santa Marta Schists, Northern Colombia: insights on the growth and approach of Cretaceous Caribbean oceanic terranes to the South American continent. Journal of South American Earth Sciences 29, 784–804.

Cardona-Molina, A., Cordani, U.G., MacDonald, W., 2006. Tectonic correlations of pre-mesozoic crust from the northern termination of the Colombian Andes, Caribbean region. Journal of South American Earth Sciences 21, 337–354.

Case, J.E., 1974. Major basin along the continental margin of Northern South America. In: Burk, C.A., C.L. (Eds.), Drake the Geology of Continental Margins. Springer Verlag, Berlin-New York, pp. 733–741.

Cawood, P.A., Kröner, A., Collins, W.J., Kusky, T.D., Mooney, W.D., Windley, B.F., 2009. Accretionary orogens through Earth history. In: Cawood, P.A., Kröner, A. (Eds.), Earth Accretionary Systems in Space and Time. Geological Society of London, pp. 1–36. Special Publication, 318.

Cerón, J., Kellogg, J., Ojeda, G., 2007. Basament configuration of the Northwestern South America-Caribbean margin from recent geophysical data. CT&F-Ciencia. Tecnología y Futuro 3 (3).

Chang, Z., Vervoort, J.D., McClelland, W.C., Knaack, C., 2006. U-Pb dating of zircon by LA-ICP-MS. Geochemistry, Geophysics, Geosystems 7, 1–14.

Colmenares, L., Zoback, M.D., 2003. Stress field and seismotectonics of northern South America. Geology 31, 721–724.

Corredor, F., 2003. Seismic strain rates and distributed continental deformation in the northern Andes and three-dimensional seismotectonics of the northwestern South America. Tectonophysics 372, 147–166.

Cortés, M., Angelier, J., 2005. Current states of stress in the northern Andes as indicated by focal mechanism of earthquakes. Tectonophysics 403, 29–58.

Cox, K., Bell, J., Pankhurst, R., 1979. The Interpretation of Igneous Rocks. George Allen y Unwin, London, 450 pp.

Crawford, A.J., Falloon, T.J., Eggins, S., 1987. The origin of island arc high-alumina basalts. Contributions to Mineralogy and Petrology 97, 417–430.

Crotwell, H.P., Owens, T.J., Ritsema, J., 1999. The Tau-P Toolkit: flexible seismic travel-time and ray-path utilities. Seismological Research Letters 70, 154–160.

Davis, A.S., Clangue, D.A., Paduan, J.B., Cousens, B.L., Huard, J., 2010. Origin of volcanic seamounts at the continental margin of California related to changes in plate margins. Geochemistry Geophysics Geosystems 11, Q05006. http://dx.doi.org/10.1029/2010GC003064.

Dickinson, W.R., 1985. Interpreting provenance relations from detrital modes of Sandstones. In: Zuffa, G.G. (Ed.), Provenance of Arenites, pp. 333–361.

Ding, X.Y., Grand, S.P., 1994. Seismic structure of the deep Kurile subduction zone. Journal of Geophysical Research 99, 23767–23786. http://dx.doi.org/10.1029/94JB02130.

Duque-Caro, H., 1984. Estilo estructural, diapirismo y episodios de acrecimiento del terreno Sinú-San Jacinto en el Noroccidente de Colombia. Ingeominas Bogotá 27 (2), 1–29.

Ellis, B., Messina, A., 1940. (et seq.) Catalogue of Foraminifera. In: The American Museum of Natural History, vol. 30 (Special Publication).

Farris, D.W., Jaramillo, C., Bayona, G., Restrepo-Moreno, S.A., Montes, C., Cardona, A., Mora, A., Speakman, R.J., Glascock, M.D., Valencia, V., 2011. Fracturing of the Panamanian Isthmus during initial collision with South America. Geology 39, 1007–1010.

Flinch, J.F., 2003. Structural evolution of the Sinu-lower Magdalena area (Northern Colombia). In: Bartolini, C., Buffler, R.T., Blickwede, J. (Eds.), The Circum-gulf of Mexico and the Caribbean: Hydrocarbon Habitats, Basin Formation, and Plate Tectonics, vol. 79. AAPG Memoir, pp. 776–796.

Flinch, J.F., Amaral, J., Doulcet, A., Mouly, B., Osorio, O., Pince, J.M., 2003. Onshore-offshore structure of the northern Colombia accretionary complex. In: AAPG International Conference. Barcelona, Spain.

Folk, R., 1980. Petrology of Sedimentary Rocks. Hemphill, Austin, Texas, 182 pp.

Gasparon, M., Rosenbaum, G., Wijbrans, J., Manetti, P., 2009. The transition subduction arc to slab tearing: evidence from Capraia Island northern tyrrhenian Sea. Journal of Geodynamics 47, 30–38.

Geermerad, J.H., Hopping, C.A., Muller, J., 1968. Palynology of Tertiary sediments from tropical areas. Review of Palaeobotany and Palynology 6, 189–348.

Gehrels, G., Valencia, V., Pullen, A., 2006. Detrital zircon geochronology by laser-ablation multicollector ICPMS at the Arizona LaserChron center. In: Olszewski, T.D. (Ed.), Geochronology Emerging Opportunities, vol. 12. Paleontological Society, pp. 67–76.

Geotec, L.T.D.A., 1997. Cartografía geológica de la región del Sinú (Noroeste de Colombia), planchas 50, 51, 59, 60, 61, 69, 70, 71, 79 y 80, 3 volúmenes (Bogotá).

Geotec, L.T.D.A., 1999. Geología de la Plancha 50 Puerto Escondido. Escala 1: 100.000. Ingeominas, Bogotá.

Geotec, L.T.D.A., 2003. Geología de los cinturones Sinú-San Jacinto. 50 Puerto Escondido, 51 Lorica, 59 Mulatos, 60 Canalete, 61 Montería, 69 Necoclí, 70 San Pedro de Urabá, 71 Planeta Rica, 79 Turbo, 80 Tierralta. Escala 1:100.000. Ingeominas, Bogotá.

Gómez, J., Nivia, A., Montes, N., Jiménez, D., Sepúlveda, M., Gaona, T., Osorio, J., Diederix, H., Mora, M., Velásquez, M., 2007. Atlas geológico de Colombia. Plancha 5-03. Escala 1:500.000. Ingeominas, Bogotá.

Guzmán, G., 2007. Stratigraphy and Sedimentary Environment and Implications in the Plato basin and the San Jacinto belt, Northwestern Colombia. Ph.D. thesis. University of Liége, Belgium, 275 pp.

Guzmán, G., Londoño, E., Serrano, B., 2004. Geología de los cinturones del Sinú, San Jacinto y borde occidental del valle inferior del Magdalena Caribe Colombiano. Escala 1:300.000. Ingeominas, Bogotá.

Haase, K.M., Mühe, R., Stoffers, P., 2000. Magmatism during extension of the lithosphere: geochemical constraints from lavas of the Shaban Deep, Northern Red Sea. Chemical Geology 166, 225–239.

Hastie, A.R., Kerr, A.C., Pearce, J.A., Mitchell, S.F., 2007. Classification of altered volcanic island arc rocks using immobile trace elements: development of the Co-Th discrimination diagram. Journal of Petrology 48, 2341–2357.

Hirano, N., Takahashi, E., Yamamoto, J., Abe, N., Ingle, S., Kaneoka, I., Kimura, I., Hirata, T., Ishii, T., Ogawa, Y., Machida, S., Suyehiro, K., 2006. Volcanism in response to plate flexure. Science 313, 1426–1428. http://dx.doi.org/10.1126/Science.1128235.

Hollings, P., Wyman, D., 2005. The geochemistry of trace elements in igneous systems: principles and examples from basaltic systems. In: Linnen, R.L., Samson, I.M. (Eds.), Rare-Element Geochemistry and Mineral Deposits, GAC Short Course Notes, vol. 17. Geological Association of Canada, pp. 1–16.

Hoorn, C., Kaandorp, M., Roele, J., 1987. Tertiary Sediments of the Usme Valley, Colombia: A Palynological and Stratigraphical Approach. University of Amsterdam, 1–15 p.

Ibañez-Mejía, M., Vinasco, C., Cardona, A., Valencia, V., Weber, M., 2010. Permian-Triassic orogenesis in the northern Andes: a record of arc magmatism, accretion, anatexis and relaxation of a continental terrane in the Proto-Andes in the wake of Pangea. Geological Society of America. Annual meeting. Paper 197-1.

Jaramillo, C.A., Ochoa, D., Contreras, L., Pagani, M., Carvajal-Ortiz, H., Pratt, L.M., Krishnan, S., Cardona, A., Romero, M., Quiroz, L., Rodriguez, G., Rueda, M.J., de la Parra, F., Moron, S., Green, W.A., Bayona, G., Montes, C., Quintero, O., Ramirez, R., Mora, G., Schouten, S., Bermudez, H., Navarrete, R., Parra, F., Alvaran, M., Osorno, J., Crowley, J.L., Valencia, V., Vervoort, J., 2010. Effects of Rapid global warming at the Paleocene-Eocene boundary on neotropical vegetation. Science 330 (6006), 957–961.

Jaramillo, C.A., Rueda, M.J., Torres, V., 2011. A palynological zonation for the Cenozoic of the Llanos and Llanos Foothills of Colombia. Palynology 35 (1), 46–84.

Kellogg, J.N., Vega, V., 1995. Tectonic development of Panama, Costa Rica, and Colombian Andes: constraints from global positioning system geodetic studies and gravity. In: Mann, P. (Ed.), Geologic and Tectonic Develompment of the Caribbean Plate Boundary in Southern Central America. Geological Society of America, pp. 75–90. Special paper, 295.

Kennett, B.L.N., Engdahl, E.R., 1991. Travel times for global earthquake location and phase identification. Geophysical Journal International 122, 429–465. http://dx.doi.org/10.1111/j.1365-246X.1991.tb06724.x.

Kennett, J.P., Srinivasan, M.S., 1983. Neogene Planktonic Foraminifera. Hutchinson Ross Publishing Company, Stroudsburg, 265 pp.

Kerr, A.C., Marriner, G.F., Tarney, J., Nivia, A., Saunders, A.D., Thirlwall, M.F., Sinton, C.W., 1997. Cretaceous basaltic terranes in western Colombia: Elemental,

chronological and Sr-Nd constraints on petrogénesis. Journal of Petrology 38, 677–702.
Kitsopoulos, K.P., 1995. The Mineralogy, Geochemistry, Physical Properties and Possible Industrial Applications of Volcanic Zeolitic Tuffs from Santorini and Polyegos Islands, Greece, PhD thesis. University of Leicester, 442pp.
Le Bas, M.J., 1962. The role of aluminium in igneous clinopyroxenes with relation to their parentage. American Journal of Science 260, 267–288.
Leterrier, J., Maury, R.C., Thonon, P., Girard, D., Marchal, M., 1982. Clinopyroxene composition as a method of identification of the magmatic affinities of paleo-volcanic series. Earth and Planetary Science Letters 59, 139–154.
Loeblich, A.R., Tappan, H., 1957. Planktonic foraminifera of Paleocene and early Eocene age from the Gulf and Atlantic Coastral Plains. In: Studies in Foraminifera, vol. 215. United States National Museum Bulletin, pp. 173–198.
Loeblich, A., Tappan, H., 1988. Foraminiferal Genera and Their Classifications, vol. 212. Van Nostrand Reinhold Co, N.Y., 970, p. 847.
Londoño, J.M., Bohorquez, O.P., Ospina, L.F., 2010. Tomografía sísmica 3D del sector de Cúcuta, Colombia [online]. bol.geol. ISSN: 0120-0283 32 (1). ISSN: 0120-0283, 107–124.
Ludwig, K.J., 2007. Isoplot 3.62. Berkeley Geochonology Center, Berkeley, Special Publication, 70 pp.
Luzieux, L.D.A., Heller, F., Spikings, R., Vallejo, C.F., Winkler, W., 2006. Origin and Cretaceous tectonic history of the coastal Ecuadorian forearc between 1°S-4°S: paleomagnetic, radiometric and fossil evidence. Earth and Planetary Science Letters 249, 400–414.
Macellari, C.E., 1984. Late Tertiary history of the Táchira depression, south-western Venezuelan Andes. In: Bonini, W.E., et al. (Eds.), The Caribbean–south American Plate Boundary and Regional Tectonics, vol. 162. Geological Society of America, Memoir, pp. 333–342.
Madsen, J.K., Thorkelson, D.J., Friedman, R.M., Marshall, D.D., 2006. Cenozoic to Recent plate configurations in the Pacific Basin: ridge subduction and slab window magmatism in western North America. Geological Society of America. Geosphere 2 (1), 11–34. http://dx.doi.org/10.1130/GES00020.1.
Mange, A.M., Maurer, W.H., 1992. Heavy Minerals in Colour. Chapman and Hall, pp. 11–28.
Mantilla-Pimiento, A., Jentzsch, G., Kley, J., Pava, A., 2009. Configuration of the Colombia Caribbean margin: constraints from 2D seismic reflection data potencial fields interpretation. In: Lallemand, S., Funiciello, F. (Eds.), Subduction Zone Geodynamics. © Springer-Verlag, Berlin Heidelberg, pp. 247–272. http://dx.doi.org/10.1007/978-3-540-87974-9.
Martinod, J., Husson, L., Roperch, P., Guillaume, B., Espurt, N., 2010. Horizontal subduction zones, convergence velocity and the building of the Andes. Earth and Planetary Science Letters 299, 299–309.
Masliwec, A., 1984. Applicability of the 40Ar/39Ar Method to the Dating of Ore Bodies. Doctoral thesis. University of Toronto, Canada, 159 pp.
Mauffret, A., Leroy, S., 1997. Seismic stratigraphy and structure of the Caribbean igneous province. Tectonophysics 283, 61–104.
Mcphie, J., Doyle, M., Allen, R., 1993. Volcanic Textures, A Guide to the Interpretation of Textures in Volcanic Rocks. University of Tasmania, Australia.
Miller, M.S., Levander, A., Niu, F., Li, A., 2009. Upper mantle structure beneath the Caribbean – south American plate boundary from surface wave tomography. Journal of Geophysical Research 114 (B01312). http://dx.doi.org/10.1029/2007JB005507.
Montes, C., Guzmán, G., Bayona, G., Cardona, A., Valencia, V., Jaramillo, C., 2010. Clockwise rotation of the Santa Marta massif and simultaneous Paleogene to Neogene deformation of the Plato-San Jorge and Cesar-Ranchería basins. Journal of South American Earth Sciences 29, 832–848.
Montes, C., Cardona, A., McFadden, R.R., Moron, S.E., Silva, C.A., Restrepo-Moreno, S.A., Ramirez, D.A., Hoyos, N., Wilson, J., Farris, D., Bayona, G.A., Jaramillo, C.A., Valencia, V., Bryan, J., Flores, J.A., 2012a. Evidence for middle Eocene and younger emergence in Central Panama: implications for Isthmus closure. Geological Society of America Bulletin 124 (5–6), 780–799.
Montes, C., Bayona, G., Cardona, A., Buchs, D., Silva, C., Moron, S.E., Hoyon, N., Ramirez, D.A., Jaramillo, C., Valencia, V., 2012b. Arc-continent collision and orocline formation: closing of the Central American Seaway. Journal of Geophysical Research 117 (B04105), 25.
Morimoto, N., Fabries, J., Ferguson, A.K., Ginzburg, I.V., Ross, M., Seifert, F.A., Zussman, J., Aoki, K., Gottardi, G., 1988. Nomenclature of pyroxenes. American Mineralogist 73, 1123–1133.
Morkhoven, F., Berggren, W., Edwards, A., 1986. Cenozoic Cosmopolitan Deep-water Benthic Foraminifera. Elf-Aquitaine, p. 421.
Muessig, K.W., 1984. Structure and Cenozoic Tectonics of the Falcón Basin, Venezuela, and Adjacent Areas, vol. 162. Geological Society of America. Memoir. 217–230.
Müller, R.D., Royer, J.Y., Cande, S.C., Roest, W.R., Maschenkov, S., 1999. New constraints on the Late Cretaceous/Tertiary Plate tectonic evolution of the Caribbean. In: Mann, P. (Ed.), Caribbean Basins: Sedimentary Basins of the World, vol. 4. Elsevier Science, Amsterdam, pp. 33–59.
Nakamura, N., 1974. Determination of REE, Ba, Fe, Mg, Na and K in carbonaceous and ordinary chondrites. Geochemical Cosmochimical Acta 38, 757–773.
Niu, Y., Wilson, M., Humphreys, E.R., O'Hara, J., 2011. The origin of intra-plate ocean island basalts (OIB): the lid effect and its geodynamic implications. Journal of Petroloy 52, 1443–1468.
Pearce, J.A., 1996. A user's guide to basalt discrimination diagrams. In: Wyman, D.A. (Ed.), Trace Element Geochemistry of Volcanic Rocks: Applications for Massive Sulphide Exploration, vol. 12. Geological Association of Canada, pp. 79–114. Short Course Notes.
Pearce, J.A., Peate, D.W., 1995. Tectonic implications of the composition of volcanic arc magmas. Annual Review of Earth and Planetary Sciences 23, 251–328. http://dx.doi.org/10.1146/annurev.ea.23.050195.001343.
Peccerillo, A., Taylor, S.R., 1976. Geochemistry of Eocene calc-alkaline volcanic rocks from the Kastamonu area, northern Turkey. Contributions to Mineralogy and Petrology 58, 63–81. http://dx.doi.org/10.1007/BF00384745.
Perez, O.J., Bilham, R., Bendick, R., Velandia, J.R., Hernandez, N., Moncayo, C., Hoyer, M., Kozuch, M., 2001. Velocity field across the southern Caribbean plate boundary and estimates of Caribbean/South-American Plate motion using GPS geodesy 1994-2000. Geophysical Research Letters 28, 2987–2990.
Pindell, J.L., Kennan, L., 2009. Tectonic Evolution of the Gulf of Mexico, Caribbean and Northern South America in the Mantle Reference Frame: An Update, vol. 328. Geological Society. Special Publications. 1–55.
Pindell, J.L., Higgs, R., Dewey, J.F., 1998. Cenozoic palinspastic reconstruction, paleogeographic evolution, and hydrocarbon setting of the northern margin of South America. In: Pindell, J.L., Drake, C.L. (Eds.), Paleogeographic Evolution and Non-glacial Eustasy, Northern South America, vol. 58. SEPM Special Publication, pp. 45–86.
Pindell, J., Kennan, L., Maresch, W.V., Stanek, K.P., Draper, G., Higgs, R., 2005. Plate kinematic and crustal dynamics of circum-Caribbean arc-Continent interactions: tectonics controls on basin development in the Proto-Caribbean margins. In: Avé Lallemant, H.G., Sisson, V.B. (Eds.), Caribbean–South American Plate Interactions, vol. 394. Geological Society of America, pp. 7–52. Special Paper.
Schoonmaker, A., Kidd, W.S.F., Bradley, D.C., 2005. Foreland-forearc collisional granitoid and mafic magmatism caused by lower-plate lithospheric slab breakoff: the Acadian of Maine, and other orogens. Geology 33 (12), 961964. http://dx.doi.org/10.1130/G21832.1.
Scrope, G.P., 1858. The Geology of Extinct Volcanoes of Central France. John Murray, London.
Shervais, J.W., 1982. Ti–V plots and the petrogenesis of modern and ophiolitic lavas. Earth and Planetary Science Letters 59, 101–118.
Silva-Caminha, S.A.F., Jaramillo, C.A., Absy, M.L., 2010. Neogene palynology of the Solimoes basin, Brazilian Amazonia. Palaeontographica, Abteilung B: Palaeobotany – Palaeophytology 283 (1–3), 1–67.
Skilling, I.P., White, J.D.L., Mcphie, J., 2002. Peperite: a review of magma–sediment mingling. Journal of Volcanology and Geothermal Research 114, 1–17.
Spadea, P., Espinosa, A., 1996. Petrology and chemistry of late Cretaceous volcanic rocks from the southernmost segment of the Western Cordillera of Colombia (South America). Journal of South American Earth Sciences 9, 79–90.
Steiger, R.H., Jäger, E., 1977. Subcommission on Geochronology: convention on the use of decay constants in geo and Cosmochronology. Earth and Planetary Sciences Letters 36, 359–362.
Sun, S., McDonough, W.F., 1989. Chemical and Isotopic Systematics of oceanic basalts: implications for Mantle Composition and Processes. In: Saunders, A.D., Norry, M.J. (Eds.), Magmatism in the Ocean Basins, vol. 42. Geological Society Special Publication, pp. 313–345.
Taboada, A., Rivera, L.,T., Fuenzalida, A., Cisternas, A., Philip, H., Bijwaard, H., Olaya, J., Rivera, C., 2000. Geodynamics of the northern Andes: subductions and intracontinental deformation (Colombia). Tectonics 19, 787–813.
Tatsumi, Y., 2005. The Subduction Factory: How It Operates in the Evolving Earth, vol. 15. Geological Society of America, Today. no 7.
Tatsumi, Y., Eggins, S., 1995. Subduction Zone Magmatism. Blackwell, Science, Boston, 211 pp.
Thorkelson, D.J., 1996. Subduction of diverging plates and the principles of slab window formation. Tectonophysics 255, 47–63.
Toto, E., Kellogg, J., 1992. Structure of the Sinú-San Jacinto fold belt: an active accretionary prism in northern Colombia. Journal of South American Earth Sciences 5, 211–222.
Traverse, A., 2007. Paleopalynology, Dordrecht, London. Topics in Geobiology 28, 236–814.
Trenkamp, R., Kellogg, J.N., Freymueller, J.T., Mora, H.P., 2002. Wide plate margin deformation, Southern Central America and northwester South America, CASA GPS observations. Journal of South American Earth Sciences 15, 157–171.
Vallejo, C., Spikings, R.A., Winkler, W., Luzieux, L., Chew, D., Page, L., 2006. The early interaction between the Caribbean Plateau and the NW South American plate. Terra Nova 18, 264–269.
Van Der Hilst, R., Mann, P., 1994. Tectonic implications of tomographic images of subducted lithosphere beneath northwestern South America. Geology 22, 451–454.
Vargas, C., Mann, P., Gomez, C., Briceño, L., Rey, C., 2010. Trans-andean mega-regional seismic reflection line extending from the Caribbean coast to cordillera Oriental of Colombia: implication for hydrocarbon exploration. In: Conference AAPG 2010 Annual Convention and Exhibition (ACE). In New Orleans, Louisiana.
Villagómez, D., Spikings, R., Magna, T., Kammer, A., Wilfried, W., Beltran, A., 2011. Geochronology, geochemistry and tectonic evolution of the Western and Central cordilleras of Colombia. Lithos 125, 875–896.
Vinasco, C.J., Cordani, U.G., González, H., Weber, M., Pelaez, C., 2006. Geochronological, isotopic, and geochemical data from Permo-Triassic granitic gneisses and granitoids of the Colombian Central Andes. Journal of South American Earth Sciences 21, 355–371.
Weber, J., Dixon, T., Demets, C., Ambeh, W., Jansma, P., Mattioli, G., Bilham, R., Saleh, J., Perez, O., 2001. A GPS estimate of the relative motion between the

Caribbean and south American plates, and geologic implications for Trinidad and Venezuela. Geology 29, 75–78.
Weber, M., Cardona, A., Paniagua, F., Cordani, U., Sepúlveda, L., Wilson, R., 2009. The Cabo de la Vela mafic-ultramafic complex, Northeastern Colombian Caribbean region – a record of multi stage evolution of a Late Cretaceous intraoceanic arc. In: The Geology and Evolution of the Region between North and South America, vol. 328. Geological Society of London, Special Publication. 549–568.
White, J.D.L., Mcphie, J., Skilling, I.P., 2000. Peperite: a useful genetic term. Bullettin of Volcanology 62, 65–66.
Wohletz, K., 2002. Water/magma interaction: some theory and experiments on peperite formation. Journal of Volcanology and Geothermal Research 114, 19–35.
Wood, D.A., 1980. The application of a Th-Hf-Ta diagram to problems of tectono-magmatic classification and to establishing the nature of crustal contamination of basaltic lavas of the British Tertiary volcanic province. Earth and Planetary Science Letters 50, 11–30.
Wortel, R., Govers, R., Spakman, W., 2009. Continental Collision and the STEP-wise Evolution of Convergent Plate Boundaries: From Structure to Dynamics. Subduction Zone Geodynamics. © Springer-Verlag, Berlin Heidelberg. http://dx.doi.org/10.1007/978-3-540-87974-9.
Yamamoto, T., Hoang, N., 2009. Synchronous Japan Sea opening Miocene fore-arc volcanism in the Abukuma Mountains, NE Japan: an advancing hot asthenosphere flow versus Pacific slab melting. Lithos 112, 575–590.
York, D., Evensen, N.M., López-Martínez, M., De Basabe- Delgado, J., 2004. Unified equations for the slope, intercept, and standard errors of the best straight line. American Journal of Physics 73, 367–375.
Zhao, J-x, McCulloch, M.T., 1993. Melting of a subduction-modified continental lithospheric mantle: evidence from Late Proterozoic mafic dike swarms in central Australia. Geology 21, 463–466.
Zhou, R., Grand, S.P., Tajima, F., Ding, X.Y., 1996. High velocity zone beneath the southern Tibetan plateau from P-wave differential travel-time data. Geophysical Research Letters 23, 25–28.